Electronic Supplementary Material (ESI) for Physical Chemistry Chemical Physics.
This journal is © the Owner Societies 2018

Optical Transient Absorption Experiments Reveal the Failure of Formal Kinetics in Diffusion Assisted Electron Transfer Reactions

Supporting Information

G. Angulo[1*], A. Rosspeintner[2*], B. Lang[2], and E. Vauthey[2]

[1]Institute of Physical Chemistry, Polish Academy of Sciences, 01-224 Warsaw, Poland
[2]Department of Physical Chemistry, University of Geneva, CH-1211 Geneva, Switzerland

Contents

List of Figures

List of Tables

1 Formal Kinetics Model

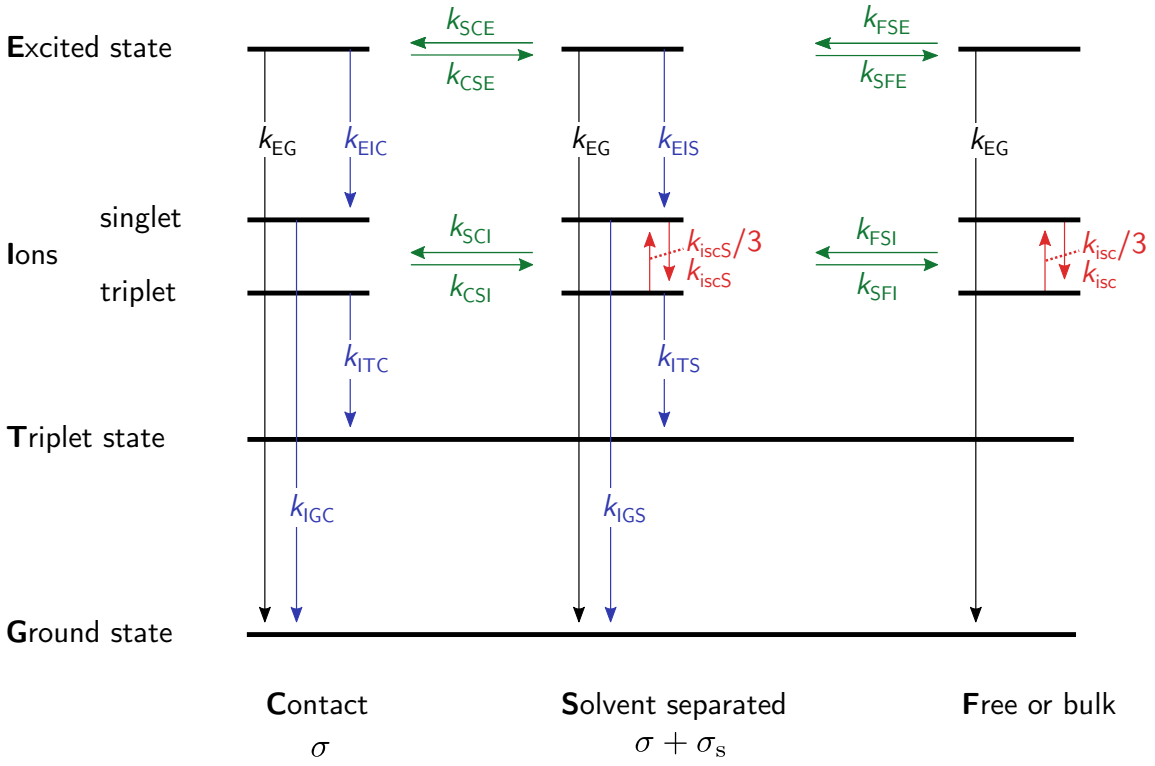

Scheme S 1: Kinetic scheme for the proposed reactions according to a consistent formal kinetics approach.

Scheme S1 explicits the formal kinetic scheme, necessary to account for a consistent inclusion of contact- (C), solvent separated-pairs (S) and free-ions (F). For 'vertical' rates the subindices of the rate constant, k_{ABC}, indicate the educt state (A), the product state (B) and the spatial position (C). Thus, for example k_{ITC} indicates the reaction from the ions to the triplet at contact. On the other hand, 'horizontal' rate subindices indicate the initial spatial position, the final spatial position, and the relevant electronic state. For example, k_{SCI} indicates diffusion from the solvent-separated to the contact ion pair. The intersystem crossing rate constant between the singlet and triplet free ions is labelled k_{isc}.
The initial condition has been chosen as follows: We assume, that at increasing quencher concentration the probability of having a quencher at distance C or S will also increase. Using the same rate constants for the ground state as for the excited state and setting the total fluorophore concentration in the solution, $[\mathrm{E_{total}}] = 10^{-5}\,\mathrm{M}$ we can see that:

$$[\mathrm{E_S}](0) = [\mathrm{E_{total}}]\frac{1}{1 + \frac{k_{\mathrm{SCE}}}{k_{\mathrm{CSE}}} + \frac{k_{\mathrm{SFE}}}{k_{\mathrm{FSE}}}} \tag{S1}$$

$$[\mathrm{E_C}](0) = [\mathrm{E_S}](0)\frac{k_{\mathrm{SCE}}}{k_{\mathrm{CSE}}} \tag{S2}$$

$$[\mathrm{E_F}](0) = [\mathrm{E_S}](0)\frac{k_{\mathrm{SFE}}}{k_{\mathrm{FSE}}}. \tag{S3}$$

Obviously, all other concentrations are zero at time zero. All adjustable parameters are summarized in Table 2.

Table S 1: Definition of the rate constants entering the formal kinetics scheme.

rate	process	expression	comment
k_{EG}	lifetime	from experiment	Inverse of fluorescence lifetime, τ_{ES}.
k_{isc}	spin conversion	unknown	Value in the bulk. This is the rate from S to T, while T to S is simply one third of this value.
k_{iscS}	spin conversion	$k_{\mathrm{isc}}/\alpha_{\mathrm{isc}}$	Value in the SSIP. α_{isc} is an attenuation factor accounting for the slowest ISC at shorter inter-radical distances. We consider the ISC to be negligible at contact.
k_{FSE}	diffusion	$4\pi D(\sigma+\sigma_{\mathrm{s}})c$	In the scheme all rate constants are monomolecular.
k_{SFE}	diffusion	$k_{\mathrm{FSE}}/(V_{\mathrm{s}}c)$	V_{s} is the volume of the SS encounter complex.
k_{SFI}	diffusion	$\frac{3r_{\mathrm{C}}D_{\mathrm{ion}}}{(\sigma+\sigma_{\mathrm{s}})^3(1-e^{-r_{\mathrm{C}}/(\sigma+\sigma_{\mathrm{s}})})}$	Commonly called k_{sep}; r_{C} is the Onsager radius with its sign. D_{ion} is smaller than D for the neutrals.
k_{FSI}	diffusion	$4\pi D_{\mathrm{ion}}\frac{r_{\mathrm{C}}}{e^{r_{\mathrm{C}}/(\sigma+\sigma_{\mathrm{s}})}-1}$	
k_{SCE}	diffusion	unknown	scaled to other solvents using the ratio of the diffusion coefficients with respect to acetonitrile.
k_{CSE}	diffusion	$k_{\mathrm{SCE}}\left(\frac{\sigma+\sigma_{\mathrm{s}}}{\sigma}\right)^3$	Comes from the equilibrium constant deduced by Shoup and Szabo.[1]
k_{SCI}	diffusion	unknown	We assume this is independent of the spin state of the ion pair.
k_{CSI}	diffusion	$k_{\mathrm{SCI}}\left(\frac{\sigma+\sigma_{\mathrm{s}}}{\sigma}\right)^3 e^{r_{\mathrm{C}}(\frac{1}{\sigma}-\frac{1}{\sigma+\sigma_{\mathrm{s}}})}$	
k_{EIC}	electron transfer	$\alpha_{\mathrm{F}}\frac{k_{0\mathrm{F}}}{1+e^{-2\sigma_{\mathrm{s}}/L_{\mathrm{F}}}}$	This and the subsequent expression come from the fact that the sum of both expressions must coincide with the integrated value of the rate obtained from UT ($k_{0\mathrm{F}}$), and that they are related to each other by the decay of the tunneling length, L_{F}. α_{F} is an adjustable parameter.
k_{EIS}	electron transfer	$k_{\mathrm{EIC}}e^{-2\sigma_{\mathrm{s}}/L_{\mathrm{F}}}$	
k_{IGC}	electron transfer	$\alpha_{\mathrm{R}}\frac{k_{0\mathrm{RS}}}{1+e^{-2\sigma_{\mathrm{s}}/L_{\mathrm{R}}}}$	
k_{IGS}	electron transfer	$k_{\mathrm{IGC}}e^{-2\sigma_{\mathrm{s}}/L_{\mathrm{R}}}$	
k_{ITC}	electron transfer	$\alpha_{\mathrm{R}}\frac{k_{0\mathrm{RT}}}{1+e^{-2\sigma_{\mathrm{s}}/L_{\mathrm{R}}}}$	
k_{ITS}	electron transfer	$k_{\mathrm{ITC}}e^{-2\sigma_{\mathrm{s}}/L_{\mathrm{R}}}$	

Table S 2: Adjustable parameters in the formal kinetic scheme.

parameter	value	**description**
k_{isc}	$0.4\,\mathrm{ns}^{-1}$	rate of intersystem crossing in the free radical ions
α_{isc}	5	attenuation factor for slower ISC in the SSIP ($\mathrm{I_S}$)
σ	$0.65\sigma_{\mathrm{UT}}$ Å	contact radius
σ_{s}	$0.75\sigma_{\mathrm{s,UT}}$ Å	solvent diameter
k_{SCE}	$6D/D(\mathrm{ACN})\,\mathrm{ns}^{-1}$	rate for interconversion from $\mathrm{E_S}$ to $\mathrm{E_C}$
k_{SCI}	$6D_{\mathrm{ion}}/D_{\mathrm{ion}}(\mathrm{ACN})\,\mathrm{ns}^{-1}$	rate for interconversion from $\mathrm{I_S}$ to $\mathrm{I_C}$
α_{F}	$2\cdot10^{-3}$ Å^{-3}	multiplicative factor for the forward ET rate constant
α_{R}	$2\cdot10^{-4}$ Å^{-3}	multiplicative factor for the recombination ET rate constant

2 Diffusion-Reaction Model

In the following, the boundary conditions and diffusion operators, $\hat{L}_x$ with $x \in \{\mathrm{I},\mathrm{R}\}$, for the various diffusion-reaction-equations given in the main manuscript are written out.[2]

2.1 Charge Separation

$$\rho^{\mathrm{ES}}(r,0) = g(r) \tag{S4a}$$

$$\rho^{\mathrm{ES}}(\infty,t) = 1 \tag{S4b}$$

$$\left(\frac{\partial\rho^{\mathrm{ES}}(r,t)}{\partial r} + \rho^{\mathrm{ES}}(r,t)\frac{\partial v_{\mathrm{I}}(r)}{\partial r}\right)\bigg|_{r=\sigma} = 0 \tag{S4c}$$

2.2 Charge Recombination

$$\rho^{\mathrm{I}}(r,0) = 0 \tag{S5a}$$

$$\left(\frac{\partial\rho^{\mathrm{I}}(r,t)}{\partial r} + \rho^{\mathrm{I}}(r,t)\frac{\partial v_{\mathrm{R}}(r)}{\partial r}\right)\bigg|_{r=\sigma} = 0 \tag{S5b}$$

The diffusion operator is given by

$$\hat{L}_{\mathrm{x}} = \frac{1}{r^2}\frac{\partial}{\partial r}r^2 D(r)\exp\left(-v_x(r)\right)\frac{\partial}{\partial r}\exp\left(v_x(r)\right), \tag{S6}$$

where the potential of mean force for the ionization (I) and recombination (R) process is given by

$$v_x(r) = \begin{cases} -\ln(g(r)) & \text{ionization, } x = \mathrm{I} \\ -\ln(g(r)) + \frac{r_{\mathrm{C}}}{r} & \text{recombination, } x = \mathrm{R} \end{cases} \tag{S7}$$

with $g(r)$ denoting the solvent-solvent pair distribution function (*vide infra*) and r_{C} is the Onsager radius given by

$$r_{\mathrm{C}} = \frac{z_1 z_2 e^2}{4\pi\epsilon_0\epsilon k_{\mathrm{B}}T} \tag{S8}$$

2.3 Diffusion Coefficient and Solvent Structure

The necessity of accounting for a distance dependent diffusion coefficient, $D(r)$, and the intrinsic structure of the solvent, via its pair distribution function $g(r)$, in the theoretical description of

bimolecular reactions in liquid solutions has been theoretically and experimentally shown by the group of Fayer and co-workers.[3,4]
Here we use the classical expression for the distance dependent diffusion coefficient, $D(r)$, of equal sized reactants[3]

$$D(r) = D_{\text{bulk}} \left(1 - \frac{3\sigma}{4r}\right). \tag{S9}$$

The solvent-solvent pair distribution function, $g(r)$, is evaluated using the Percus Yevick equation requiring as input the solvent diameter, σ_{solv}, the mass density, ρ, the molar mass, M_{w} and the packing fraction, $P = \pi\rho\sigma_{\text{solv}}^3 N_{\text{A}}/(6M_{\text{w}})$.

3 Electron Transfer Equations

The following equations apply for solutes of identical size, i.e. $r_\mathrm{D} = r_\mathrm{A} = \sigma/2$, and redox potentials, $E(\dots)$, determined in a solvent of dielectric constant ϵ_ref.

- distance dependence of solvent reorganization energy

$$\lambda_\mathrm{s}(r) = \frac{e^2}{4\pi\epsilon_0}\left(\frac{1}{n^2} - \frac{1}{\epsilon}\right)\left(2 - \frac{\sigma}{r}\right) \tag{S10}$$

- distance dependence of reaction free energies

$$\Delta G_\mathrm{I}(r) = \Delta G(\sigma) + \frac{k_\mathrm{B}Tr_\mathrm{C}}{r} \tag{S11a}$$

$$\Delta G_\mathrm{RS}(r) = -\Delta G(\sigma) - \frac{k_\mathrm{B}Tr_\mathrm{C}}{r} - E_{00} \tag{S11b}$$

$$\Delta G_\mathrm{RT}(r) = -\Delta G(\sigma) - \frac{k_\mathrm{B}Tr_\mathrm{C}}{r} - E_{00} + E_\mathrm{T} \tag{S11c}$$

  where

$$\Delta G(\sigma) = E(\mathrm{D}^+/\mathrm{D}) - E(\mathrm{A}/\mathrm{A}^-) - E_{00} - \frac{e^2}{2\pi\epsilon_0\sigma}\left(\frac{1}{\epsilon_\mathrm{ref}} - \frac{1}{\epsilon}\right) \tag{S12}$$

- distance dependence of the Levich-Dogonadze preexponential factor, $U_x(r)$ (with $x \in \{\mathrm{I}, \mathrm{RS}, \mathrm{RT}\}$

$$U_x(r) = V_x^2 e^{-2(r-\sigma)/L_x}\sqrt{\frac{\pi}{\hbar^2 k_\mathrm{B}T\lambda_\mathrm{s}(r)}} \tag{S13}$$

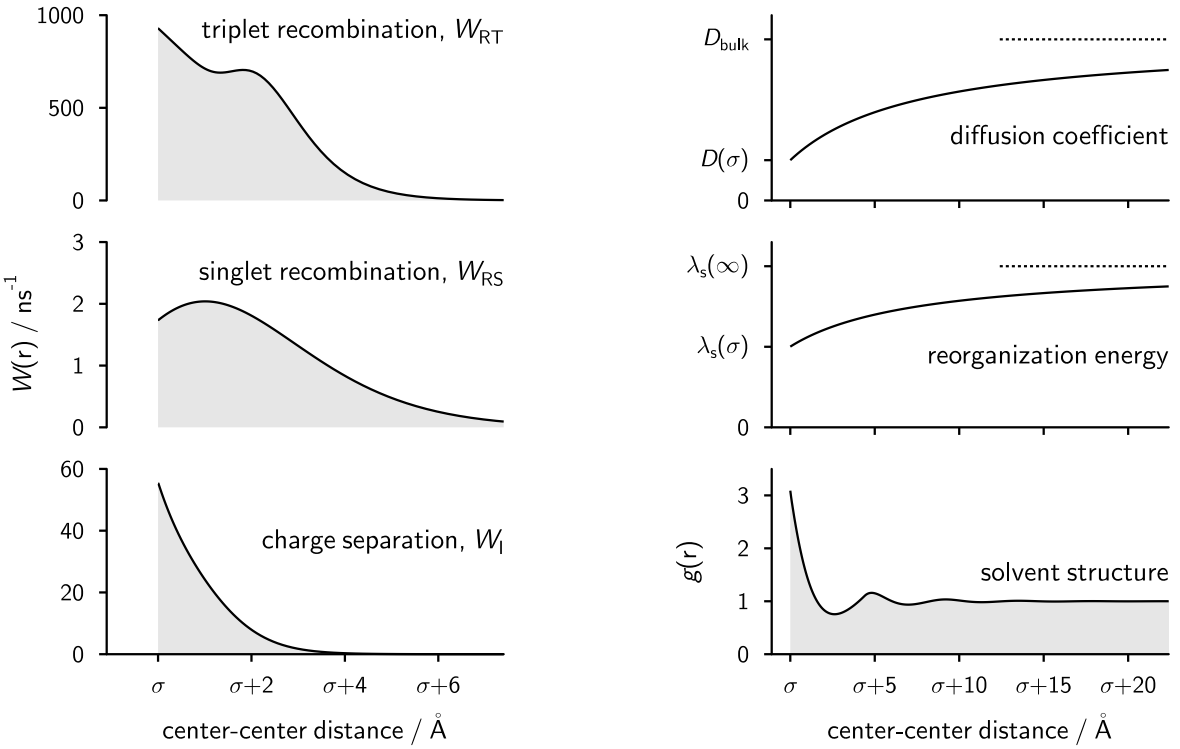

(a) Distance dependence of reaction probabilities in dimethylsulfoxide

(b) Distance dependence of solvent structure, reorganization energy and diffusion coefficient

Figure S 1: Distance dependence of relevant quantities for the diffusion-reaction equation approach.

4 Diffusion Reaction Model Parameters

Table S 3: Parameters used in the diffusion reaction model.

solvent	E_{00} [eV]	σ [Å]	σ_s [Å]	V_I [meV]	V_{RS} [meV]	V_{RT} [meV]	L_I [Å]	L_{RS} [Å]	L_{RT} [Å]	λ_q [eV]	$\hbar\omega$ [eV]	W_{ST} [ns^{-1}]	L_{ST} [Å]	τ_L [ps]
ACN	2.93	7.50	3.0					1.9		0.175		0.038		0.55
DMF	2.83	7.75	4.0					1.9		0.170		0.030		0.75
DMSO	2.83	7.60	4.4					2.0		0.185		0.030		0.65
DG4	2.83	7.70	4.4					2.0		0.185		0.030		0.65
DG8	2.83	7.75	4.4	40	53	50	1.5	2.0	1.7	0.185	0.186	0.030	2.0	0.65
DG16	2.83	7.85	4.4					2.0		0.185		0.015		0.65
DG32	2.83	8.00	4.4					2.0		0.185		0.015		0.65
DG64	2.83	8.15	4.4					2.0		0.185		0.012		0.65
DG100	2.83	8.15	4.4					2.0		0.185		0.009		0.65

5 Effect of Infinitely Fast / Slow Diffusion

The kinetic traces for the excited state and the total population of the ions at very large and very small diffusion coefficients compared to the one in acetonitrile, can help visualizing when diffusion starts to affect the populations. In figure S2 it can be observed that the deviations between the three cases are noticeable already between 10 and 100 ps. In the case of no movement no free ions are created, all recombine and the quenching is overall much slower. In the other extreme almost all created ions can escape and the quenching is faster than in ACN. The case of a vanishingly small diffusion coefficient is equivalent to a solid. It is important to note, that despite the absence of diffusion the reactant and product distributions still play a crucial role. It would not be enough to consider a simple rate constant based model as can be seen from the shape of the ions kinetics. In the case of pure "kinetic control", when diffusion is much faster than any other process things are simpler and the kinetics reflect quite well the nature of the electron transfer reaction itself. Still, even in this case, the distance dependence of the reactivity is mixed with the solvent structure and a formal kinetics approach would require introducing several states to explain the kinetics. Moreover, the example shown is for a single quencher concentration only. The quencher concentration dependence of both, quenching and recombination can not be properly explained by a formal kinetic model in any case, except maybe for the extremely high diffusion coefficient.

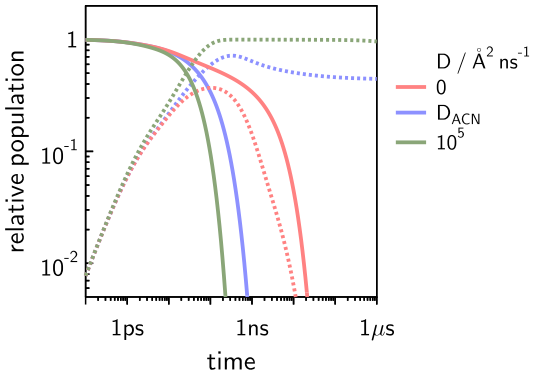

Figure S 2: Comparison of the simulated kinetics assuming three different diffusion coefficients, two of which representing extreme cases, i.e. no diffusion and extremely fast diffusion. Solid lines denote the kinetics of the **Pe** excited state, while dashed lines are the kinetics of the ion pair.

6 Examples of Solutions to the Diffusion-Reaction Equations

Figures 3a and 3b show the solutions to eqs. 18, 19, 24 and 25 of the main MS, i.e. the pair distribution function of the excited singlet state and the ion pair. In addition, the subpopulations of the singlet and triplet radical ion pairs are shown. To visualize the effect of the recombination reaction, the ion pair distribution functions are also shown in the absence of any charge recombination reaction.

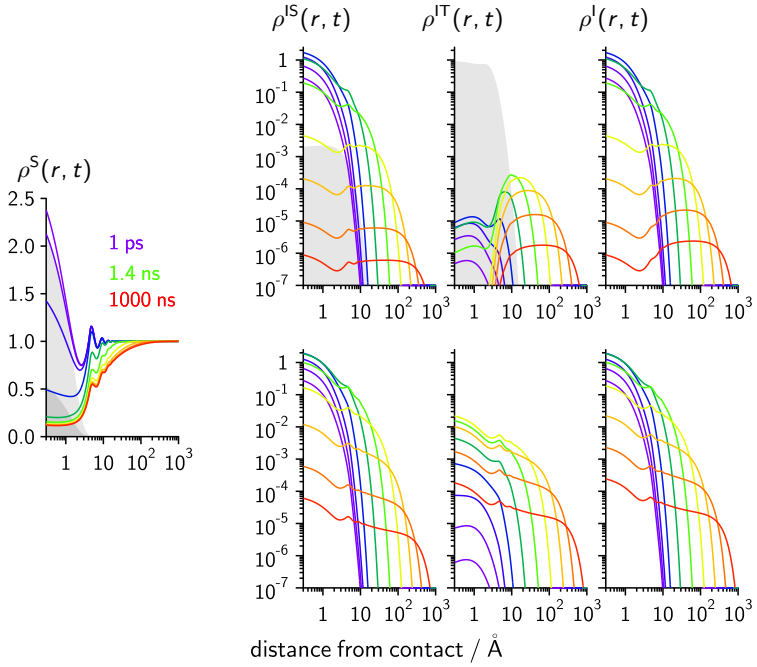

(a) Pair distribution functions for **Pe**/**DMA** at 2 cP

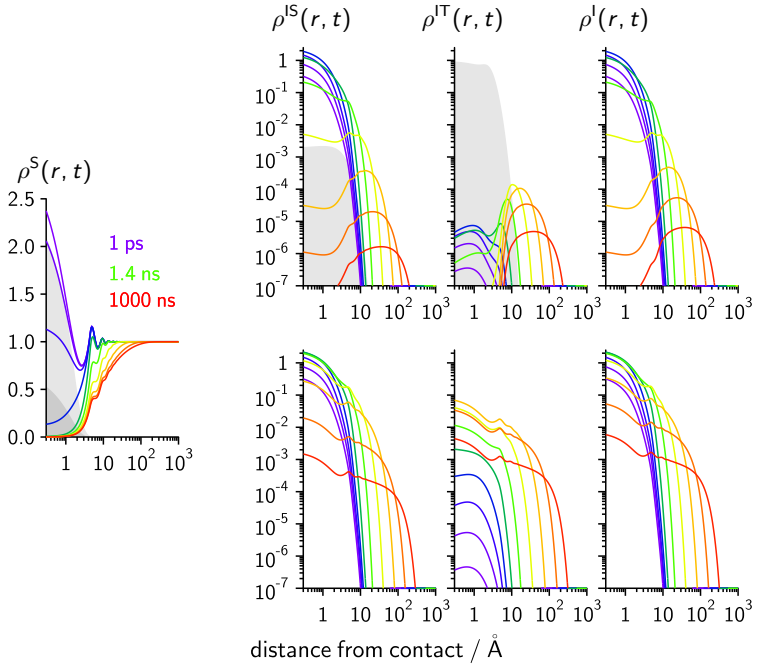

(b) Pair distribution functions for **Pe**/**DMA** at 16 cP

Figure S 3: Pair distribution functions of the singlet excited state, ρ^{S}, the total ion pair, ρ^{I}, and it's singlet, ρ^{IS}, and triplet, ρ^{IT}, subpopulations when charge recombination is allowed (upper panel) or switched off (lower panel) in a solvent of 2.2 (a) and 16 cP (b). Grey areas denote the reaction probabilities, $W_X(r)$, similar to Fig. S1a. Note that only the relative scaling among the W_{I}s and the W_{R}s is correct.

7 Experimental Details

Chemicals. Acetonitrile (ACN, Roth, Rotidry, $\geq$ 99.9%), dimethylformamide (DMF, Acros, 99.8+%, spectroscopic grade), dimethylsulfoxide (DMSO, Fisher Scientific, U.K., 99.7%) and glycerol (GLY, Alfa Aesar, ultrapure, HPLC grade) were used as received. DMSO and GLY were stored under argon.
Perylene (**Pe**, Sigma Aldrich, sublimed grade, $\geq$ 99.5%) was sublimed under reduced pressure. N,N-dimethylaniline (**DMA**, Fluka, puriss p.a., 99.5%) was distilled under reduced pressure and stored in the dark under argon.

Table S 4: Composition and basic macroscopic properties (viscosity, η, refractive index, n_D, and dielectric constant, ϵ) of the solvents used. In addition the **DMA** concentration of each measured sample is given (c_x, columns 5-7), as well as the fluorescence lifetime of **Pe**, τ_{ES}. The concentration of **Pe** for TA measurements was in the range of 25 μM.

sample[a]	η [cP]	n_D	ϵ	c_1 [M]	c_2 [M]	c_3 [M]	τ_{ES} [ns]
ACN (acetonitrile)	0.34[b]	1.34[b]	35.9[b]	0.10	0.30	0.80	5.6
DMF (dimethylformamide)	0.92[c]	1.43[b]	36.7[b]	0.10	0.30	0.80	5.1
DMSO (dimethylsulfoxide)[d]	2.2	1.48	45.9	0.10	0.32	0.82	4.9
DG4 ($x_{GLY} = 0.10$)	4.0	1.48	49.6	0.10	0.30	0.80	4.9
DG8 ($x_{GLY} = 0.22$)	8.0	1.48	51.8	0.10	0.31	0.80	4.9
DG16 ($x_{GLY} = 0.33$)	15.8	1.48	52.3	0.10	0.30	0.76	4.9
DG32 ($x_{GLY} = 0.44$)	32.7	1.48	51.5	0.10	0.33	0.80	4.9
DG64 ($x_{GLY} = 0.55$)	64	1.48	50.0	0.11	0.30	n.m.	4.8
DG100 ($x_{GLY} = 0.62$)	103	1.48	48.7	0.10	0.30	n.m.	4.9

[a] samples DGX denote binary mixtures of dimethylsulfoxide / glycerol with an approximate viscosity of X cP. [b] from ref. 5 [c] from ref. 6 [d] all data from ref. 7

Steady-State Measurements. Absorption spectra were measured on a Cary 50 spectrometer.

Time Correlated Single Photon Counting. Nanosecond, single-wavelength, time-resolved fluorescence experiments were performed using a home-built time-correlated single-photon-counting setup described in the supplementary material of ref. 8. In brief, the sample was excited at 395 nm using a pulsed laser diode (Picoquant, LDH-P-C-405) with an approximate pulse duration of 50 ps. The time-resolution of these experiments, as judged from the full-width half maximum of the instrument response function (IRF), measured with a dilute scattering solution of Ludox in water, amounts to approximately 200 ps. The emission was recorded passing through a foil-polarizer at magic angle with respect to the vertically polarized excitation and an interference filter appropriate for observing the central part of the emission spectrum (467 nm). The lifetimes of **Pe** in all solvents are given in Tab. S4.

Transient Absorption spectroscopy. TA measurements were performed with two pump-probe setups. The fs-ps TA setup used to record spectra up to 1.5 ns with a wavelength dependent IRF of ca. 100-350 fs (fwhm) are described in detail elsewhere.[9] Excitation was performed using 400 nm pulses generated by frequency doubling part of the output of a standard 1 kHz Ti:Sapphire amplified system (Spectra Physics, Spitfire). The fluence of the pump pulses on the sample was ca. 0.2-0.4 mJ/cm^2. The signal obtained from the fs-experiments was checked prior to the experiment to scale linearly with the pump energy. In order to compensate for pump beam divergence and/or delay-line misalignment, the fs-TA dynamics were corrected by comparing with a calibration sample of the pure **Pe**-decay measured on the TA and the TCSPC set-up.

The ns-μs TA setup, used to record spectra up to 500 ns with an IRF of 350 ps (fwhm) has been described in detail in ref. 10. Excitation was performed at 355 nm using a passively Q-switched, frequency doubled Nd:YAG laser (Teem Photonics, Powerchip NanoUV) producing pulses with 500 Hz repetition rate, approximately 20 μJ energy per pulse, and 300 ps duration. The pump fluence on the sample was in the range from 0.4-2 $^{mJ}/_{cm^2}$.
In both setups, probing was achieved using white light pulses generated by focusing 800 nm pulses in a CaF_2 plate. The polarization of the pump pulses was set to magic angle relative to the white-light pulses. All transient absorption spectra were corrected for background signals showing up before time zero (e. g. spontaneous emission), and - if necessary - for the dispersion due to the optical chirp. Both TA set-ups yielded - almost to within experimental uncertainty - identical transient difference spectra (see Fig. S6).
The sample solutions were located in 1 mm quartz cuvettes (Starna, model 1GS/Q/1) and bubbled with nitrogen during the measurements. When necessary - at higher viscosities - the samples were additionally stirred with a Teflon stirrer during the measurement to refresh the sample volume in the excitation spot. For the ns-experiments, the sample volume was additionally purged with nitrogen for at least 10 minutes prior to each measurement. During the measurement (with or without stirring) the cuvette was 'sealed' by a continuous nitrogen flow. The absorbance of the sample at the excitation wavelength was 0.22-0.33 (at 400 nm) and 0.06-0.07 (at 355 nm) on 1 mm. The absorption spectra of all samples before and after the transient absorption experiments showed no signs of degradation.

Diffusion-ordered NMR spectroscopy (DOSY) Experiments. DOSY experiments at 293 K were performed following the procedure outlined in ref. 7. Further details on the diffusion coefficients are collected in section 8.

8 Diffusion Coefficients

The Stokes-Einstein equation constitutes a rather rough estimate for the diffusion coefficient, D_{ij}, of a spherical solute i with radius, r_i, in a given solvent of viscosity η_j

$$D_{ij} = \frac{k_\mathrm{B}T}{\zeta_{ij}} = \frac{k_\mathrm{B}T}{C\pi\eta_j r_i} \tag{S14}$$

where C is a constant which depends on the boundary conditions used ($C_\mathrm{stick} = 6$, $C_\mathrm{slip} = 4$). Given the set of experimentally determined diffusion coefficient/viscosity pairs we opted for a parametrization of these data using a fractional Stokes-Einstein expression[11] for the two solutes in the used solvent (mixtures):

$$\frac{D_{ij}}{T} = \frac{k_\mathrm{B}}{C\pi r_i}\eta_j^{\beta}. \tag{S15}$$

Apart of the power-law dependence on the viscosity we assume identical C for both molecules which is tantamount to attributing all changes in the slope to differences in the molecular radii.

Table S5: Experimental diffusion coefficients, D, of **Pe** and **DMA** in solvents of varying viscosity, η.

solute	solvent	method	T [K]	η [cP]	D_bulk [Å^2/ns]	ref.
Pe	acetonitrile	capillary diffusion	298.15	0.334	225	12
	acetone	Taylor dispersion	298.15	0.325	202	13
	toluene		298.15	0.592	129	13
	cyclohexane		298.15	0.887	98	13
	DMF	chronoamperometry	298.15	0.802	80	14
	DMSO		298.15	1.99	34.2	14
	DMSO	DOSY	293.15	2.2	30.4	this work
	DG		293.15	5.0	13.8	this work
	DG		293.15	9.4	8.5	this work
	DG		293.15	25.1	2.8	this work
DMA	acetonitrile	DOSY	298.15	0.34	323	15
	cyclohexane		298.15	0.9	163	15
	EG		298.15	16.0	8.2	15
	EGG		298.15	29	3.9	15
	EGG		298.15	51	2.7	15
	EGG		298.15	135	1.3	15
	DMSO		293.15	2.2	49.2	this work
	DG		293.15	5.0	25.3	this work
	DG		293.15	9.4	16.0	this work
	DG		293.15	25.1	5.9	this work

[a] DG . . . binary mixtures of dimethylsulfoxide (DMSO) / glycerol; EGG . . . binary mixtures of ethylene glycol (EG) / glycerol

The different diffusion coefficients for neutral and ionic species can be rationalized applying Zwanzig's continuum theory,[16] where the friction, ζ, has been split into a viscous drag, ζ_v, and dielectric friction part, ζ_D.

$$\zeta_{\mathrm{v},ij} = 4\pi\eta_j r_i \tag{S16a}$$

$$\zeta_{\mathrm{D},ij} = \frac{3}{4}\frac{z^2(\epsilon - n^2)}{r_i^3\epsilon(1+2\epsilon)}\tau_{\mathrm{D},j} \tag{S16b}$$

$$D_j = \frac{k_\mathrm{B}T}{\sum_i \zeta_{\mathrm{v},ij} + \zeta_{\mathrm{D},ij}} \tag{S16c}$$

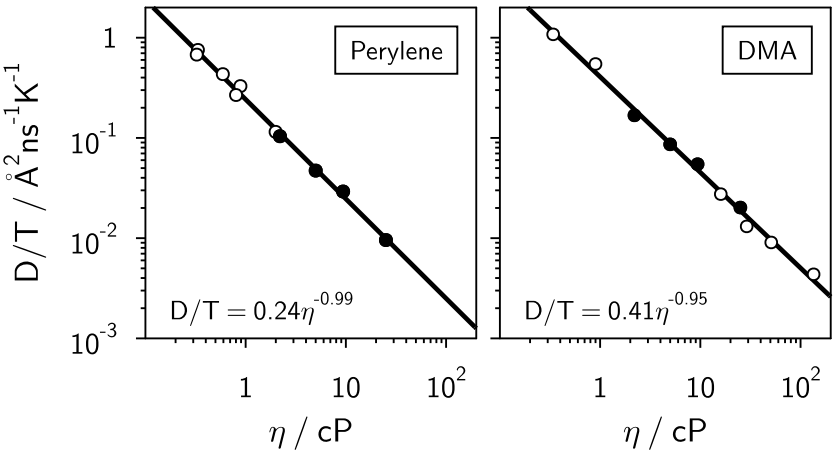

Figure S 4: Fits to the experimental dependence of D/T with viscosity, η for **Pe** and **DMA** using the data in Table S5. Open circles denote literature data, while full circles were measured in this work.

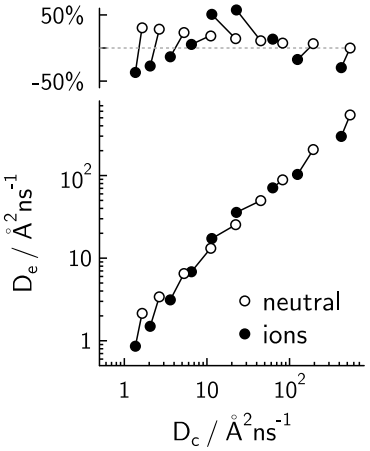

Figure S 5: Relation of measured, D_e, and calculated, D_c, diffusion coefficients for neutral educts and the ion pair (points pertaining to a single solvent are connected). For the calculations $r_{\mathbf{Pe}}$ was assumed to be 1.7 times larger than $r_{\mathbf{DMA}}$, i.e. all differences in the measured diffusion coefficients were attributed to different molecular radii.

9 Comparison of Transient Absorption-setups

As outlined in the experimental section of the main manuscript we have performed transient absorption spectra on two different set-ups. Apart of the time-resolution and the attainable maximum time-range, the main difference of these two set-ups is given by the way the whitelight continuum is focused into the sample-cell. While in the fs-TA system a thin quartz lens is used suffering from chromatic aberrations, an achromatic lens is used on the ns-TA set-up. These distorting effects due to chromatic aberration on the fs-TA can be reduced by choosing a significantly larger spot size of the pump beam than for the whitelight. By comparing the fs- and ns-TA data, with distortion effects being absent in the latter, we can judge the quality of the fs-TA spectra. In fact, Fig. S6 shows that properly chosen working conditions can alleviate the shortcomings of the fs-TA setup and render the results on the two set-ups virtually identical.

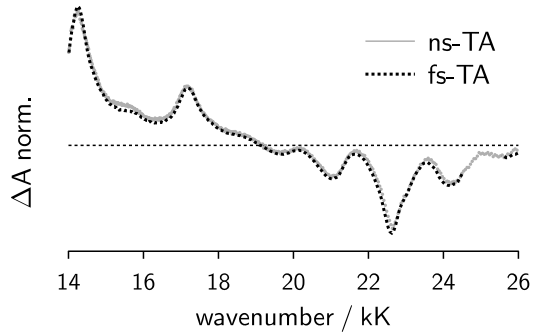

Figure S 6: Comparison of transient absorption spectra of **Pe** and 0.1 M **DMA** in dimethylsulfoxide at a time-delay of 1.3 ns recorded on the ns-TA and the fs-TA set-up. Note, that the data around 25 kK in the fs-TA data are not shown due to contamination from the pump-pulse scatter.

10 Potential Pitfalls

10.1 Spectral Overlap and Consequences for Population Dynamics

Similar, though slightly simpler approaches than the one in the main manuscript to account for overlapping dynamics have been performed in refs. 17,18. Therein the overlapping ESA contribution of the ES at the ion observation wavelength was accounted for by describing it with the (scaled) fluorescence survival probability (or population dynamics).
Fig. S8 gives an example of the flawed kinetics, if the transient absorption signal at the ion band maximum was picked as a direct marker for the ion population instead of the properly extracted ion population. Comparison of (a) and (b) clearly shows that

- the correction procedure is always necessary if correct short-time dynamics are required
- the errors introduced by residual ESA contributions are the larger the lower the quencher concentration and the higher the viscosity (i.e. the longer the ES is populated)

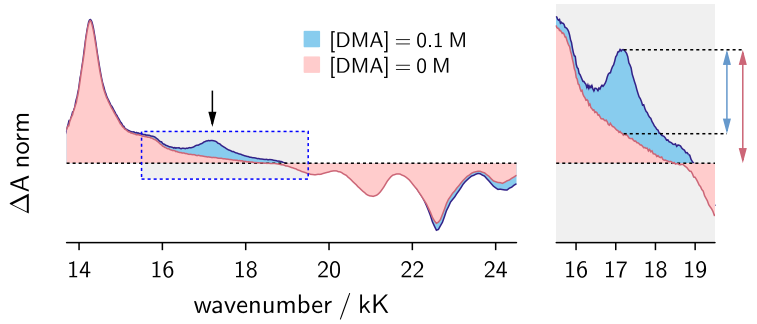

Figure S 7: Example TA spectra in DMSO/GLY (η = 32 cP) of **Pe** and **DMA** showing the effect of spectral overlap at the **Pe**-anion band (17.2 kK) at a time delay of 10^3 ps.

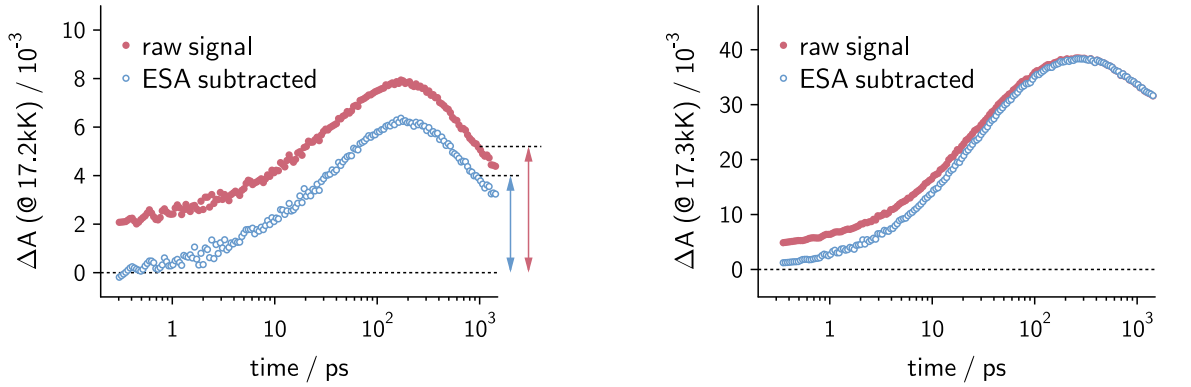

(a) 0.1 M **DMA** in DMSO/GLY (η = 32 cP)

(b) 0.8 M **DMA** in dimethylformamide (η = 0.9 cP)

Figure S 8: Comparison of the dynamics extracted at the maximum of the **Pe**-anion band position simply using the transient absorption signal (raw signal) and the signal corrected by the properly scaled **Pe**-ESA contribution at that wavenumber. (a) and (b) show the effect of the correction under different conditions (quencher concentration and viscosity).

10.2 Spectral Dynamics and Consequences for Population Dynamics

As pointed out in the main manuscript, both the **Pe**-ES (cf. Fig. S9a) as well as the transient **Pe**-anion spectra (cf. Fig. S9b) exhibit distinct spectral dynamics. It is thus obvious that the concentration of the corresponding species can *not* be extracted reliably monitoring its time-dependence at a single wavenumber. Fig. S10 compares the intrinsic **Pe**-ESA dynamics (which ideally should follow a monoexponential population decay, with τ_{ES}) when monitored via the ESA absorption maximum or the corresponding integrated band area. Clearly the deviations from ideal behaviour at short times, when spectral dynamics are prevailing, are significantly smaller for the band-area approach.
Note, however, that these intrinsic dynamics in the **Pe**-ES do not at all affect the method of obtaining the ES-population in the presence of quencher. Here, the ESA spectra of the pure **Pe** sample at the very same time-delay were applied to directly obtain the relative change in **Pe**-ES population, i.e. $p_{ES}(t)$. Nonetheless, for the ion dynamics the "integrated band area" approach will be the more reliable choice.

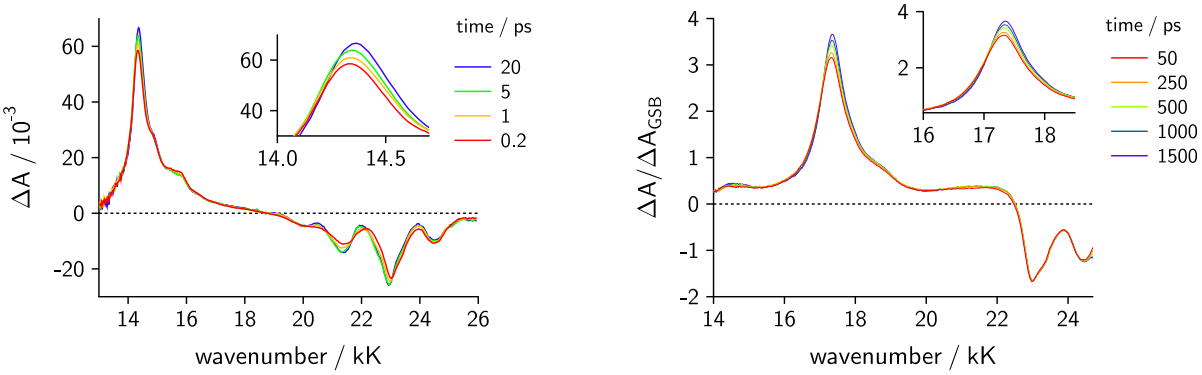

(a) Selected fs-TA spectra of **Pe** in acetonitrile **(b)** Selected fs-TA spectra of the **Pe**-anion in acetonitrile

Figure S 9: Spectral dynamics of the **Pe**-ESA in acetonitrile (left) and the **Pe**-anion generated upon photoinduced electron transfer from **DMA** in acetonitrile. The anion dynamics are scaled to afford equal ground state bleach for all times.

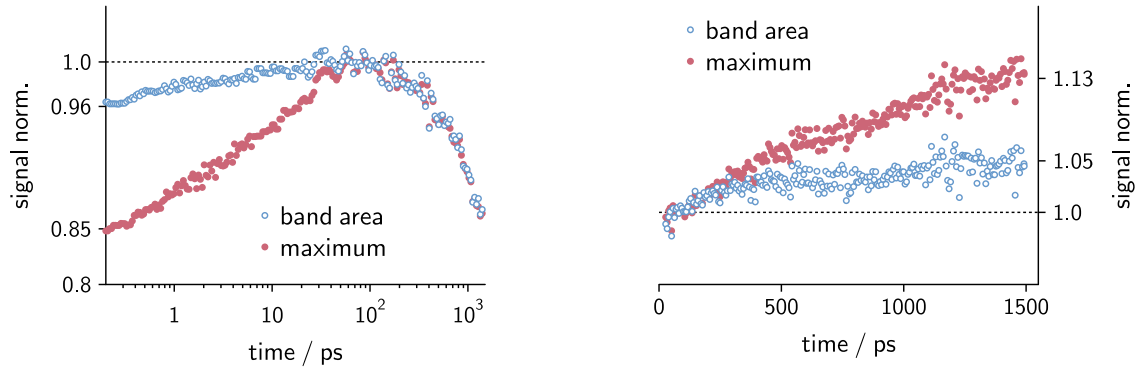

(a) **Pe**-ESA dynamics **(b)** **Pe**-anion dynamics

Figure S 10: Picosecond time evolution of the (a) **Pe**-ESA and (b) -anion band maximum and band area (13-17 kK / 16-18.5 kK, respectively) in acetonitrile. Note, that for the band area the ESA dynamics approximate the ideal monoexponential population decay significantly better than when using the band maximum.

11 Spectra

11.1 Antecedents of Perylene

Even for such a rather well-studied system as **Pe** the published extinction coefficients for ground state, excited state absorption of the singlet state (ES), the anion (I) and the triplet-triplet absorption (ET) are either relatively scarce (ESA, triplet) and/or vary greatly (anion). Table S6 lists a selection of this data and shows, that the spread is significant enough to justify a reassessment of the relevant quantities.

Table S 6: Maximum extinction coefficients of **Pe**-species from literature at the corresponding wavelengths.

species	$10^{-3}\epsilon$ [$M^{-1}cm^{-1}$]	λ [nm]	solvent	ref.	note
Pe	32	434	alcohol	19	larger value (63) at 408nm
	39.5	435	heptane	20	
	37	437	cyclohexane	21	
	32	435	cyclohexane	22	
Pe-ESA	53	700	cyclohexane	23	
	17	710	toluene	24	
Pe-triplet	14.3	490	benzene	25	vs. benzophenone ketyl ($\epsilon = 3700$)
	13	480	cyclohexane	26	vs. anthracene ($\epsilon = 64700$ at 425nm)[a]
	14	482	acetonitrile	27	vs. tetracene ($\epsilon = 31200$ at 465nm)[b]
Pe-anion	42	581	THF	28	reduction with metal
	77	579	THF	29	pulse radiolysis
	50.5	578	DMF	30	electrochemical
	56	578	DMF	30	electrochemical

[a] Ref. 31 lists a spread of this value from 25000 to more than 85000
[b] Ref. 31 lists a spread of this value from 31200 to 90000

11.1.1 Absorption Spectrum

The spread in the molar extinction coefficient of **Pe** found in the literature is close to $\pm 10\,\%$ (cf. Tab. S6). We determined the maximum ϵ for **Pe** in the lowest energy electronic absorption band in acetonitrile, DMF and dimethylsulfoxide to be $34500 \pm 500\,{}^{L}/_{\text{mol cm}}$.

11.1.2 Excited State Absorption

The transient absorption spectrum of **Pe** obtained in this work deviates significantly from the one published by Meyer and Plaza, both in terms of bandshape and maximum extinction coefficient.[23] Despite these obvious differences (shown in Fig. S11) we are confident that the data in the present work are correct for two reasons: First, the ESA spectrum of **Pe** in cyclohexane is in reasonably good agreement with data published by Dobryakov and Ernsting (cf. Fig. S11a).[32] Second, the ESA spectra measured on the fs- and ns-TA set-up are almost identical (cf. Fig. S11b).

11.1.3 (Transient) Anion Spectrum

The transient ion-pair (i.e. $\mathbf{Pe}^{\bullet -}$ / $\mathbf{DMA}^{\bullet +}$) spectrum in DMF can be compared with the electrochemically generated **Pe**-anion spectrum in the same solvent.[30] Fig. S12 shows, that the agreement in terms of bandshape is almost excellent, while the maximum absolute cross-section is slightly larger in the present case than in ref. 30. The spread for the extinction coefficient of

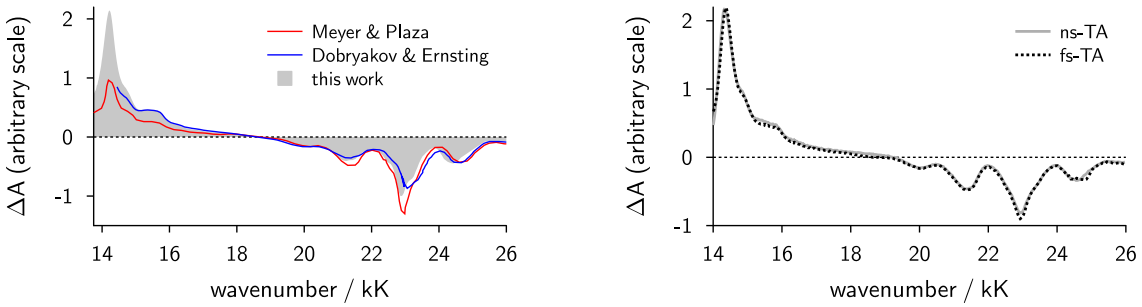

(a) **Pe**-ESA spectra in cyclohexane (normalized to the 2nd vibronic transition of the ground state bleach)

(b) Long time **Pe**-ESA spectra in acetonitrile on the fs- and ns-TA

Figure S 11: Comparison of **Pe**-ESA spectra obtained (a) at short times (1-2 ps) in different research groups[23,32] and (b) at long (1 ns) time on two different set-ups.

the **Pe**-anion in the selection of published data (cf. Table S6) is significant (up to a factor of 2) making a redetermination necessary.

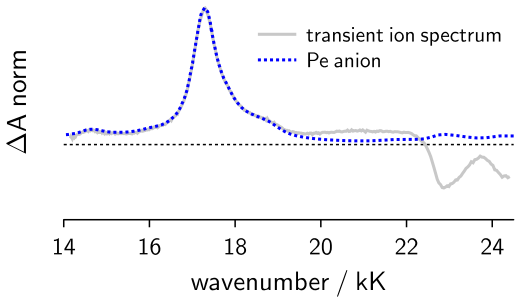

Figure S 12: Comparison of the normalized transient absorption spectrum of the ion-pair after 10 ns (grey) with the electrochemically generated **Pe**-anion spectrum (blue dashed line) from ref. 30. The positive deviation between 19-22.5 kK is due to the **DMA**-cation spectrum, while the negative feature above 22.5 kK is due to the **Pe** ground state bleach.

11.1.4 Triplet-Triplet Absorption Spectrum

Table S6 shows that the maximum triplet-triplet extinction coefficients for **Pe**, given in the literature, are surprisingly close to each other. However, closer inspection of the spread in the extinction coefficients of the used reference systems renders this data highly uncertain. Nonetheless, the experimental evidence from the literature[27,33,34], indicating that the **Pe**-triplet state does not absorb below 18 kK, can be used to obtain the triplet-triplet absorption spectrum, $\Delta A_{\mathrm{ET}}(\tilde{\nu})$, from any ns-TA spectrotemporal matrix in the presence of quencher

$$\Delta A_{\mathrm{ET}}(\tilde{\nu}) = \Delta A(c, t_2, \tilde{\nu})_{\mathrm{norm}} - \Delta A(c, t_1, \tilde{\nu})_{\mathrm{norm}}. \tag{S17}$$

Here t_1 and t_2 correspond to two time-delays sufficiently long in order to have no contribution from the **Pe**-ESA, and the normalization is performed on the **Pe**-anion peak, where the triplet-triplet absorption spectrum is expected to be zero (cf. Fig. S13a).
The so obtained bandshape of the triplet-triplet difference absorption spectrum resembles the literature data.[27,34] While the agreement with the spectrum in ref. 27 is reasonably good (in terms of bandshape), the spectrum given in ref. 34 seems to be red-shifted by approx. 0.7 kK.

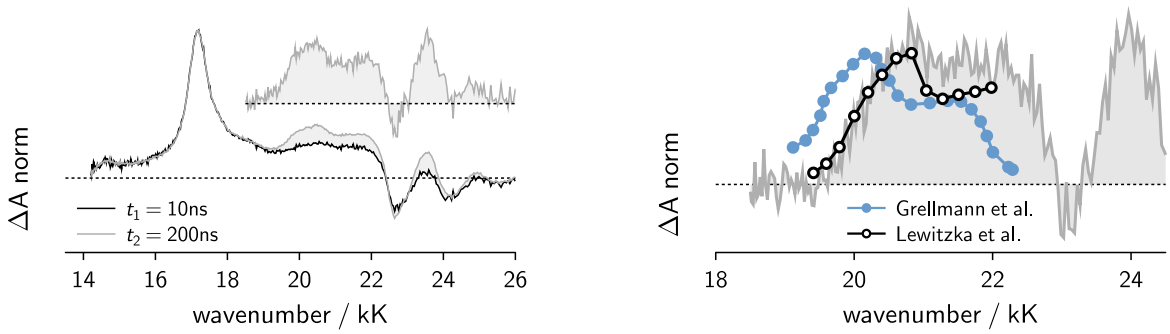

(a) Obtaining the T-T difference absorption spectrum (inset) of **Pe** in DMSO/GLY ($\eta = 8$ cP)

(b) Comparing the T-T absorption spectrum in acetonitrile with literature data

Figure S 13: (a) Procedure for obtaining the triplet-triplet difference absorption spectrum of **Pe** and (b) comparison with the bandshapes from refs. 34 (full blue circles) and 27 (open black circles).

11.1.5 Singlet and Triplet Energies

The singlet energy, E_{00}, of **Pe** is approximated by the energy of the lowest energy vibronic transition of the absorption spectrum and is in perfect agreement with previous data.[35] The triplet energy of **Pe** with $E_T = 1.55$ eV has been taken from ref. 35. This value is within the estimated range of 1.41-1.83 eV obtained in ref. 36 and very close to the one obtained experimentally in crystalline **Pe** (1.53 eV)[37] and that calculated in ref. 38 (1.57 eV) and has been heavily cited in reviews (see refs. 33,35,39,40).

11.2 Band integration ranges

Fig. S14 graphically presents the spectral ranges chosen for the spectral decomposition outlined in the main manuscript. They were chosen such as to allow for an optimal separation of the prominent optical features in the species of interest.

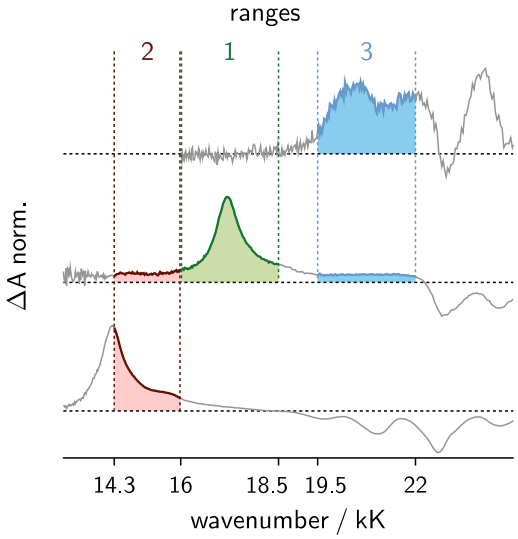

Figure S 14: Employed ranges for the constrained spectral decomposition, exemplified with the individual (vertically offset) spectral species in dimethylsulfoxide.

11.3 Extinction coefficients of transient species

11.3.1 How to get them

The extinction coefficient of transient species X can be determined using the spectral information of the difference transient absorption spectra, $\Delta A_X(\tilde{\nu})$, and the ground state extinction coefficient spectrum of **Pe**, $\epsilon_{\mathbf{Pe}}(\tilde{\nu})$,

$$\Delta\epsilon_X(\tilde{\nu}) = f_{\text{scale}}\Delta A_X(\tilde{\nu}) + \epsilon_{\mathbf{Pe}}(\tilde{\nu}), \tag{S18}$$

where the scaling factor, f_{scale}, is chosen such, that the resulting spectrum does not exhibit any spectral structure resembling that of **Pe**.[1] Fig. S15a shows the input and resulting spectra for a selected solvent.
Fig. S15b represents the resulting triplet-triplet absorption spectrum if the corresponding triplet extinction coefficient from the literature was correct. It is evident, that the so obtained triplet-triplet absorption spectrum contains a significant amount of **Pe** ground state absorption features (see red dashed lines).

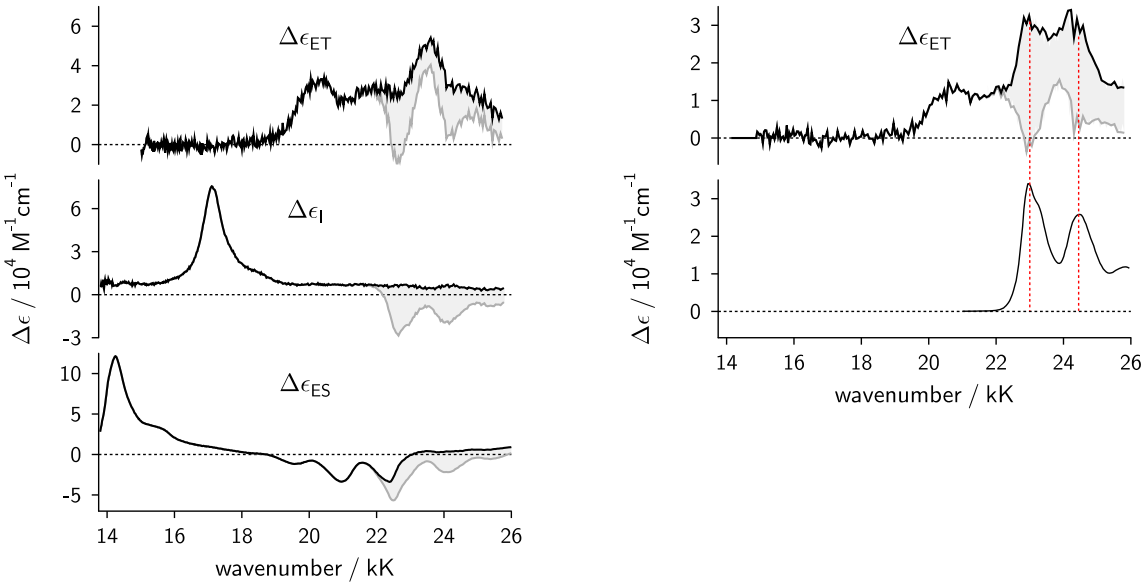

(a) Triplet-triplet (above), ion (middle) and singlet excited state (below) difference spectra in dimethylsulfoxide

(b) Triplet-triplet absorption spectrum of **Pe** (above) using the literature extinction coefficient in acetonitrile and the **Pe** absorption spectrum (middle)

Figure S15: (a) Scaled difference absorption spectra (grey), $f_{\text{scale}}\Delta A_X(\tilde{\nu})$, of the relaxed species and the ensuing extinction coefficient spectrum (black), $\Delta\epsilon_X(\tilde{\nu})$, corrected for the ground state bleach (grey filled area), $\epsilon_{\mathbf{Pe}}(\tilde{\nu})$. (b) **Pe**-triplet triplet absorption spectrum, assuming the published extinction coefficient is correct.

Table S7 and Fig. S16 demonstrate that not only does the ratio of the ESA and ion band integral not change by more than 10% among all solvents, but that the same is also true for the absolute band areas.

11.3.2 Testing them

A straightforward test of the obtained extinction coefficients consists in plotting the individual relative concentrations (or yields) and their sum, during the duration of e.g. the fs-TA experi-

[1] Wilcken et al.[41] recently used a similar approach. There the authors compared the 2$^{\text{nd}}$ derivatives of the GS and the transient absorption spectra to judge "complete GSB filling", which should be the method of choice, especially when the spectral features are relatively weak.

Table S 7: Table with extinction coefficients, ϵ_X, and the corresponding wavenumber, $\tilde{\nu}_X$. For ES the spectrally relaxed spectrum, obtained from a monoexponential global fit to the ns-TA data of a solution only containing **Pe**, was used. All ion spectra are obtained at a time-delay of 1 ns, i.e. do not necessarily pertain to the "relaxed" ion spectrum. For the triplet spectrum the two time-delays defined in eq. (S17) are given. These values have been calculated using the maximum extinction coefficient of **Pe** in its lowest electronic transition to be 34000 $^{\mathrm{L}}/_{\mathrm{mol\ cm}}$.

solvent	$10^{-4} \cdot \epsilon_{\mathrm{ES}}$ $[\mathrm{M^{-1}cm^{-1}}]$	$\tilde{\nu}_{\mathrm{ES}}$ [kK]	$10^{-4} \cdot \epsilon_{\mathrm{I}}$ $[\mathrm{M^{-1}cm^{-1}}]$	$\tilde{\nu}_{\mathrm{I}}$ [kK]	$10^{-4} \cdot \epsilon_{\mathrm{ET}}$ $[\mathrm{M^{-1}cm^{-1}}]$	$\tilde{\nu}_{\mathrm{ET}}$ [kK]	t_1 [ns]	t_2 [ns]
ACN	12.14	14.4	6.54	17.4	3.8	20.8	10	30
DMF	14.17	14.3	7.56	17.3	3.4	20.7	5	50
DMSO	12.14	14.3	7.55	17.2	3.4	20.6	20	70
DG4	12.14	14.3	7.06	17.2	3.4	20.6	20	200
DG8	11.90	14.3	7.06	17.2	3.4	20.6	10	200
DG16	12.75	14.3	6.80	17.2	3.4	20.6	10	100
DG32	12.14	14.3	6.80	17.2	3.4	20.6	10	200
DG64	12.14	14.3	6.80	17.2	3.4	20.6	10	400
DG100	13.08	14.3	6.18	17.2	3.4	20.6	20	200

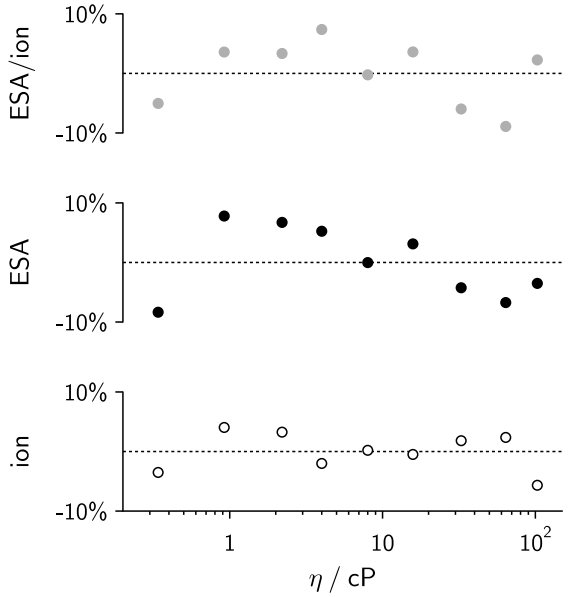

Figure S 16: ESA- (•, 13.5-18 kK) and ion-peak (○, 16-18.5 kK) areas, as well as their ratio (•), divided by the corresponding mean of all solvents.

ment. For the given reactant pair ultrafast recombination of the generated ion pair can be safely excluded, given the large energy gap, ΔG_{RS}. Thus, if the extinction coefficients of the transient species (and so their concentrations) are correct, the sum of them should be equal to 1 for all different concentrations, until charge recombination sets in. In fact, in Fig. S17 this behavior can be observed for all solvents and quencher concentrations used.

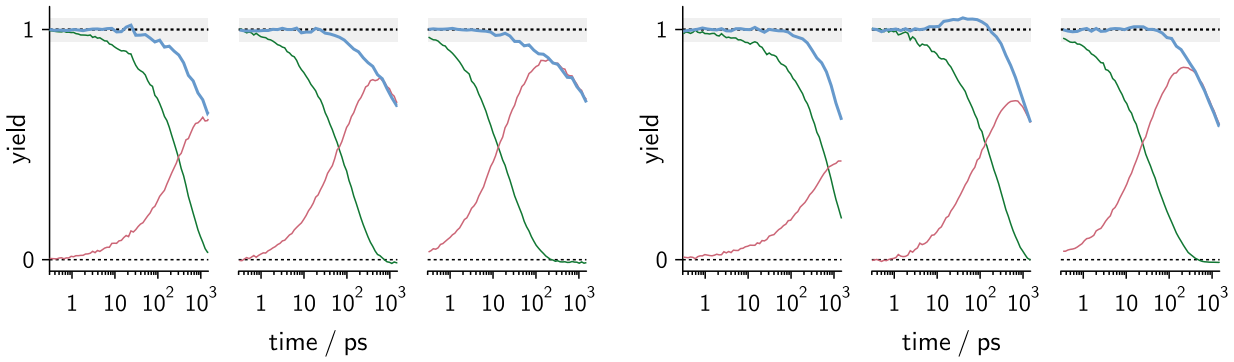

(a) acetonitrile

(b) dimethylformamide

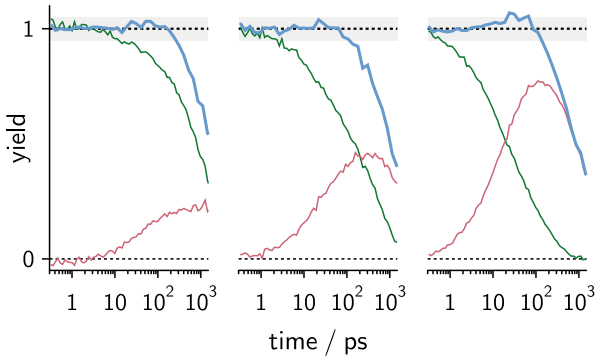

(c) dimethylsulfoxide

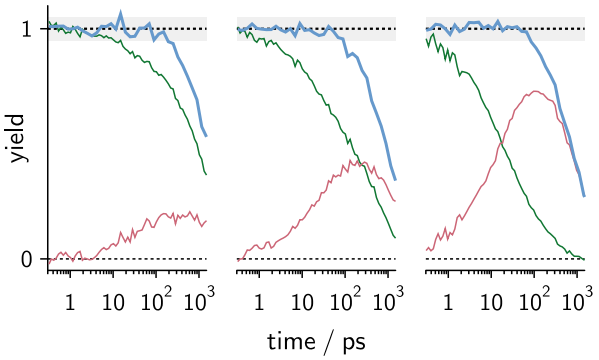

(d) DMSO/GLY ($\eta = 4\,\mathrm{cP}$)

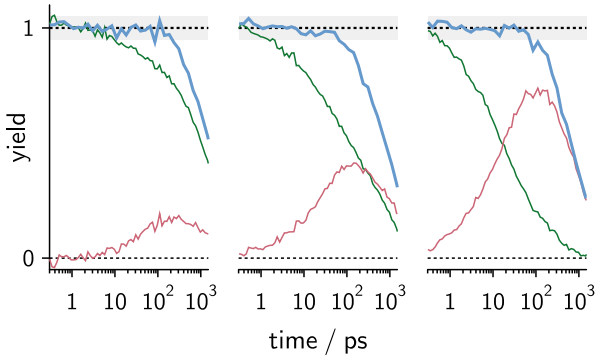

(e) DMSO/GLY ($\eta = 8\,\mathrm{cP}$)

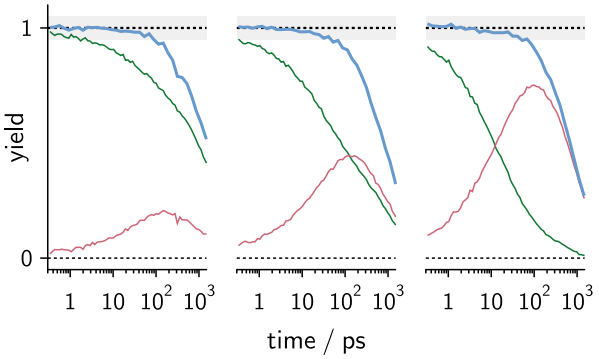

(f) DMSO/GLY ($\eta = 16\,\mathrm{cP}$)

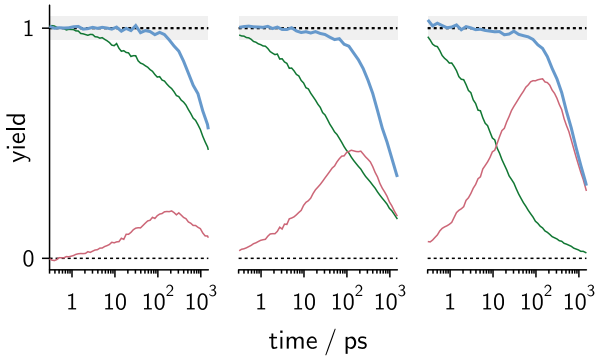

(g) DMSO/GLY ($\eta = 32\,\mathrm{cP}$)

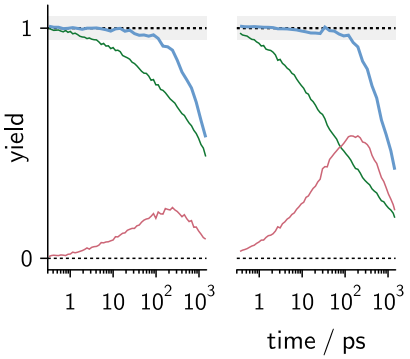

(h) DMSO/GLY ($\eta = 64\,\mathrm{cP}$)

Figure S 17: Picosecond dynamics of the yields of ES (green) and I (red) dynamics, as well as their sum (blue). The grey area around 1 indicates a range of ±5%.

12 Excited State Dynamics of Perylene

12.1 Intramolecular Vibrational Redistribution, τ_v

Previous experiments[42–44] indicate that intramolecular vibrational redistribution (IVR) in **Pe** from the $v' = 1$ excited state of a strongly Franck-Condon active ring-breathing mode[42] takes place on the time-scale of 1-2 ps and is rather solvent independent.
Here, we too have analyzed the short time-behaviour of **Pe** in all solvents studied. To this end we have focused on the wavenumber range between 19.5-24 kK, which essentially displays **Pe** ground state bleach (GSB) and stimulated emission (SE) with only a small and spectrally flat overlying excited state absorption (see Fig. S9a). Fig. S18 shows difference fs-transient absorption spectra, where the spectrum at time t has been subtracted from a spectrum at a time, when all spectral dynamics in the observation window have ceased. These (flipped) difference spectra are very similar to the time-resolved difference emission spectra in ref. 42.

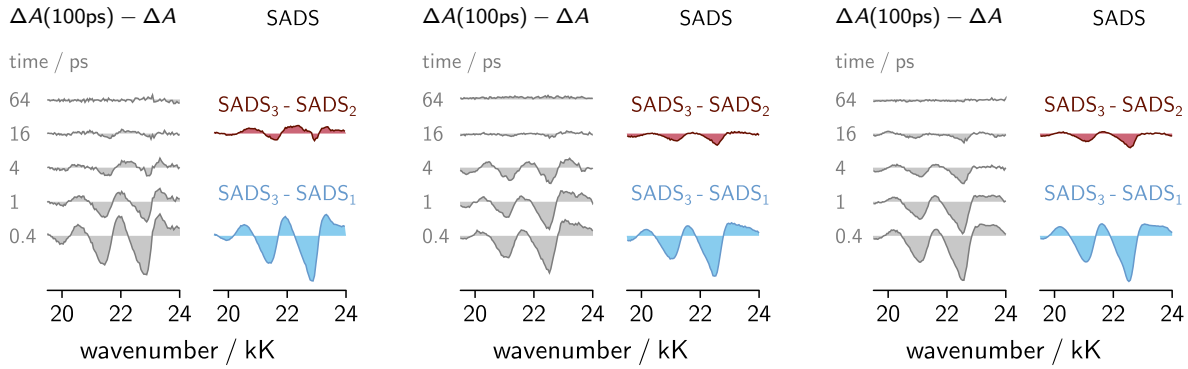

(a) acetonitrile **(b)** dimethylsulfoxide **(c)** DG32

Figure S 18: Difference fs-TA spectra at selected time-steps (left panel) and difference SADS (with $SADS_3$ being the SADS of the population decay, right panel) of **Pe** in three selected solvents.

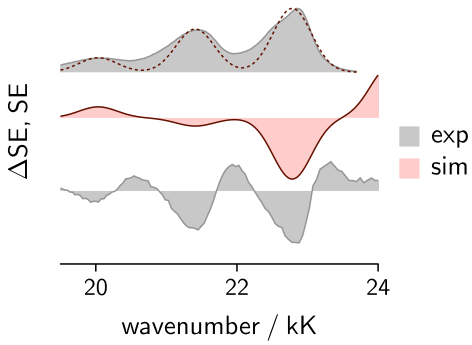

Figure S19: Comparison of experimental (grey) and simulated (red) stimulated emission spectra (upper panel) and difference spectra (lower two panels). The upper panel shows the experimental and simulated SE spectrum, σ_{SE}, (converted from the steady-state emission spectrum, $I(\tilde{\nu})$, via $\sigma_{SE}(\tilde{\nu}) = I(\tilde{\nu})/\tilde{\nu}^2$)[45], while the two lower panels show the experimental and simulated difference SE spectra.

In fact, following the formalism in ref. 42 we have also simulated the bandshape of the difference stimulated emission spectrum and compared it to our experiment (cf. Fig. S19). Given the

significant oversimplifaction by using a displaced harmonic oscillator with a single high frequency mode the essential features of the difference spectra are - at least - qualitatively reproduced.

$$\sigma_{\mathrm{SE}}(\tilde{\nu}) = \tilde{\nu} \sum_n F_{m,n} \exp\left(-\frac{(\tilde{\nu} - \tilde{\nu}_{00} + (n-m)\tilde{\nu}_{\mathrm{vib}})^2}{\sigma}\right), \tag{S19}$$

where $F_{m,n}$ is defined in eq. 31 of the main manuscript. For the simulation in Fig. S19 we used the following parameters: $\tilde{\nu}_{00} = 22.78\,\mathrm{kK}$, $\tilde{\nu}_{\mathrm{vib}} = 1.375\,\mathrm{kK}$, $\sigma = 0.15\,\mathrm{kK}^2$, $S = 0.72$. Beware that much more accurate methods for the calculation of vibrationally excited stimulated emission spectra of **Pe** have been presented.[46]

In order to estimate the population decay from the vibrationally excited state we performed a global sequential target analysis to the fs-TA data in the limited wavenumber range.[2] Then we assign the lifetime associated to the shortest, large amplitude SADS, as the lifetime of the $v' = 1$ vibrationally excited state of **Pe**. This lifetime with

$$\tau_{\mathrm{v}} = 1.8 \pm 0.2\,\mathrm{ps}$$

is almost the same in all solvents studied and does not show a trend with solvent viscosity, which is in perfect agreement with the results from refs. 42–44.

12.2 Effect of τ_{v} on the Dynamics

If the excitation energy is considerably larger than that of the 0-0 transition of the fluorophore, promoting it to vibrational states higher than the lowest one, a correction to the fluorophore kinetics taking into account the modification of the free energy of the quenching can be taken into account by introducing the relaxation time of this higher state. This part of the scheme is:

$$\begin{aligned}
N_2 &\xrightarrow{\tau_{\mathrm{v}}} N_1 && \text{vibrational relaxation}\\
N_1 &\xrightarrow{\tau_{\mathrm{F}}} N && \text{electronic relaxation}\\
N_2 + Q &\xrightarrow{k_2(t)} A^{\bullet-} + D^{\bullet+} && \text{quenching of high vibrational state}\\
N_1 + Q &\xrightarrow{k_1(t)} A^{\bullet-} + D^{\bullet+} && \text{quenching of low vibrational state}
\end{aligned}$$

Q is in large excess, N_2 is initially populated and N_1 is not. The ensuing kinetic equation for the excited states are:

$$\frac{\mathrm{d}N_2(t)}{\mathrm{d}t} = -\frac{1}{\tau_{\mathrm{v}}} N_2(t) - c k_2(t) N_2 \qquad N_2(0) = N_0 \tag{S20}$$

$$\frac{\mathrm{d}N_1(t)}{\mathrm{d}t} = \frac{1}{\tau_{\mathrm{v}}} N_2(t) - \left(\frac{1}{\tau_{\mathrm{F}}} + c k_1(t)\right) N_1(t) \qquad N_1(0) = 0. \tag{S21}$$

The solution to this set of equations is given by expressions (20) in the main manuscript.

In order to exemplify the effect of the inclusion of an excited vibrational state of **Pe** on the kinetics of the reaction with **DMA**, we have performed simulations with a very fast relaxation time ($\tau_{\mathrm{v}} = 0$) and a very slow one ($\tau_{\mathrm{v}} \to \infty$), and compared them with the simulation actually contrasted with the measurements, for the case of acetonitrile at a quencher concentration of 0.8 M. As Fig. S20 shows, the effect is not negligible at short times both in the quenching of the excited state and in the creation of the ions. At times long enough there is no appreciable effect on the kinetics of the ions.

[2] Note, that the limited window is essential, as the **Pe** excited state spectrum with it's maximum around 17.3 kK exhibits significantly longer dynamics (cf. Fig. S10a), which may have their origin in vibrational cooling.

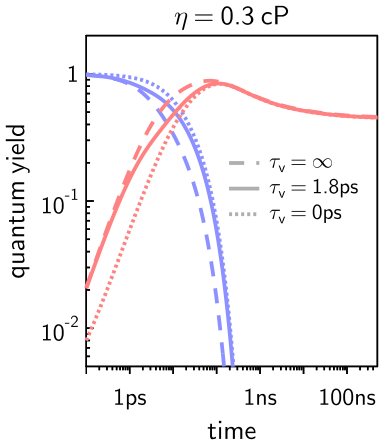

Figure S 20: Effect of reaction from a vibrationally excited state and the IVR lifetime on the kinetics of the excited state and the ions.

12.3 Vibrational Cooling

Fig. S21 shows how the ESA band of **Pe** changes with time in all solvents. We have represented the first and second moments of this band, roughly speaking equivalent to its position and its width (see eq. (S23)). As can be seen from the first moment, there are two well-separated time scales: the short one is identical to the one we have assigned to IVR just before, while the second one is in the range of 10-20 ps. Both processes seem to be independent of the solvent. The second moment, on the other hand, mostly shows the second, longer time, relaxation process. In our opinion, although not proven, this second phenomenon seems to be related to vibrational cooling. We have not found it necessary to take the dynamics of this second process into account for the reaction kinetics with **DMA**.

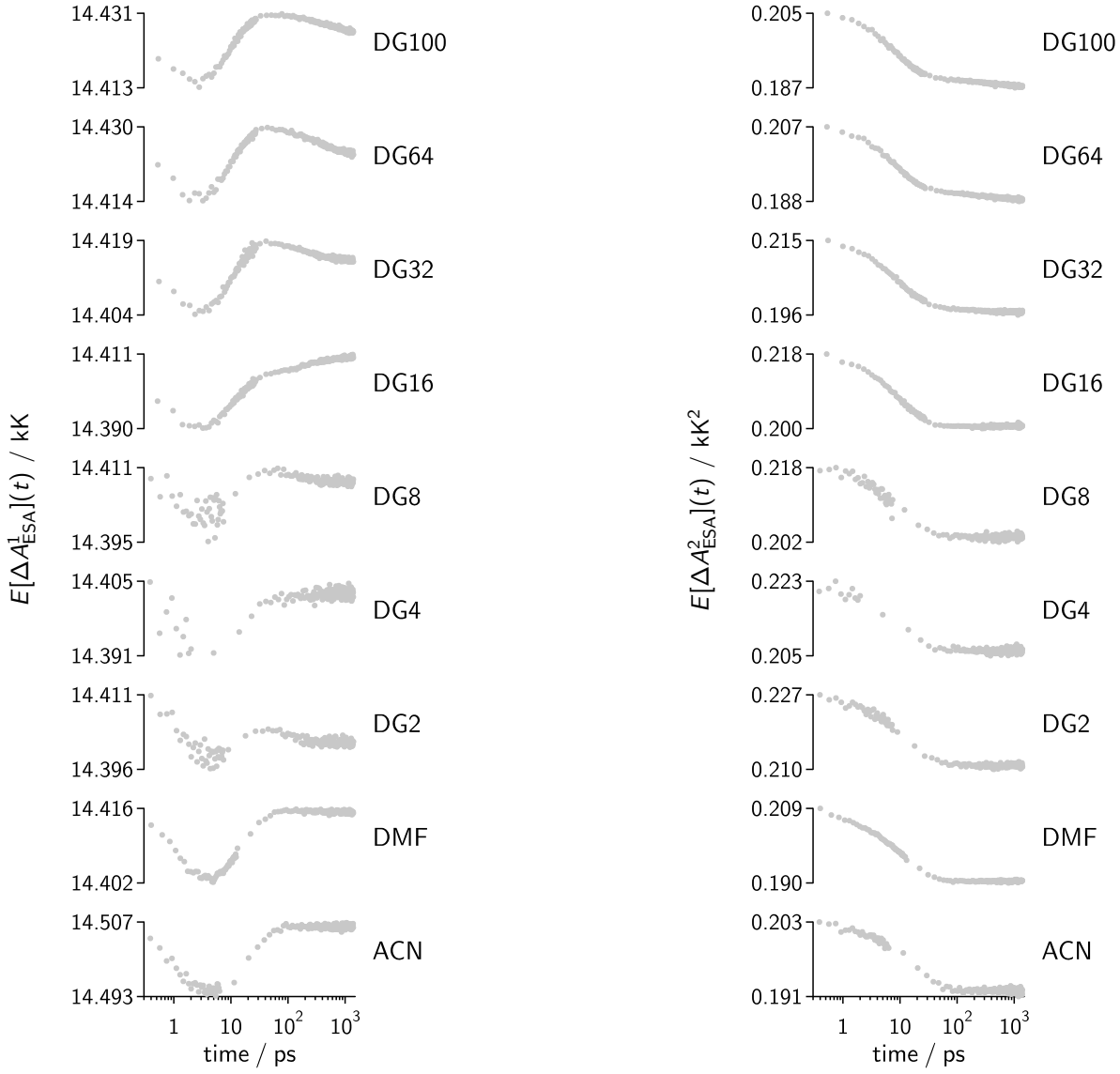

(a) 1st moments

(b) 2nd moments

Figure S 21: First (left) and second (right) moments of the **Pe** excited state absorption in the absence of quencher. The moments were calculated in the spectral range from 13.5-15.5 kK. The reduced point density is due to the fact, that in order to improve the S/N ratio the mean of 9 time-steps was taken.

13 Kinetics

13.1 Charge Separation Kinetics

Fig. S22 shows the collected population dynamics of the **Pe** excited state, $P^{\mathrm{ES}}(t)$, given by

$$P^{\mathrm{ES}}(t) = \exp\Big(-\frac{t}{\tau_{\mathrm{ES}}} - c \underbrace{\int_0^t k(t')\mathrm{d}t'}_{R(t)} \Big). \tag{S22}$$

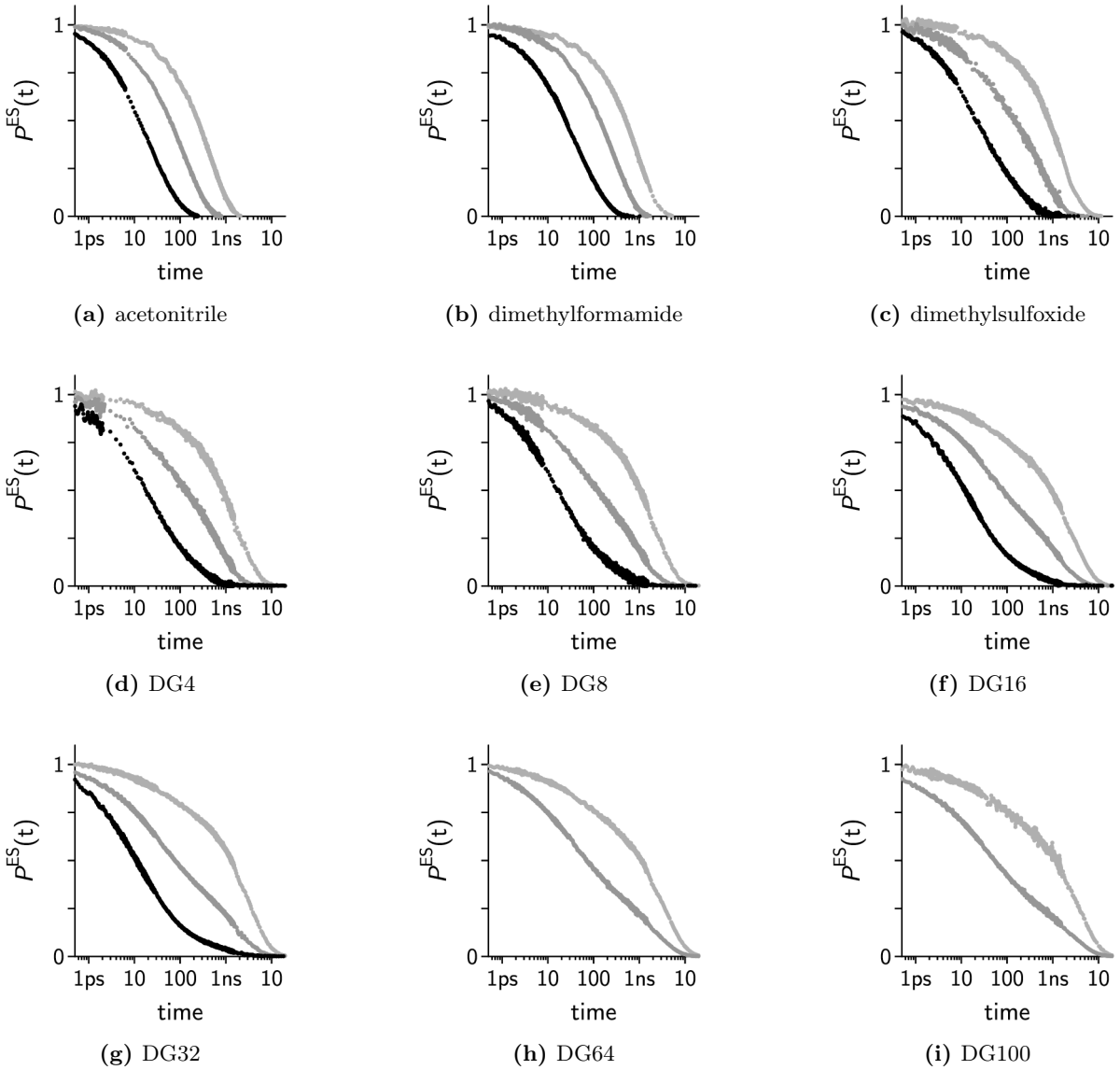

(a) acetonitrile **(b)** dimethylformamide **(c)** dimethylsulfoxide

(d) DG4 **(e)** DG8 **(f)** DG16

(g) DG32 **(h)** DG64 **(i)** DG100

Figure S 22: Excited singlet state dynamics of **Pe** as a function of quencher concentration. •. . . 0.8 M, •. . . 0.3 M, •. . . 0.1 M, denote the quenching dynamics at decreasing quencher concentration.

The time-integrated rate coefficient, $R(t)$, which - within the theoretical model used here - is supposed to be a quencher concentration independent quantity. Thus, explicitly expressing $R(t)$ and presenting it for different quencher concentrations, c, allows insight into the limitations of the applied model. In Fig. S23 the $R(t)$ dynamics in all nine solvents at three different

quencher concentrations are shown to coincide within experimental error. The TA data have been supplemented by the $R(t)$ obtained from TCSPC at the lowest quencher concentration.

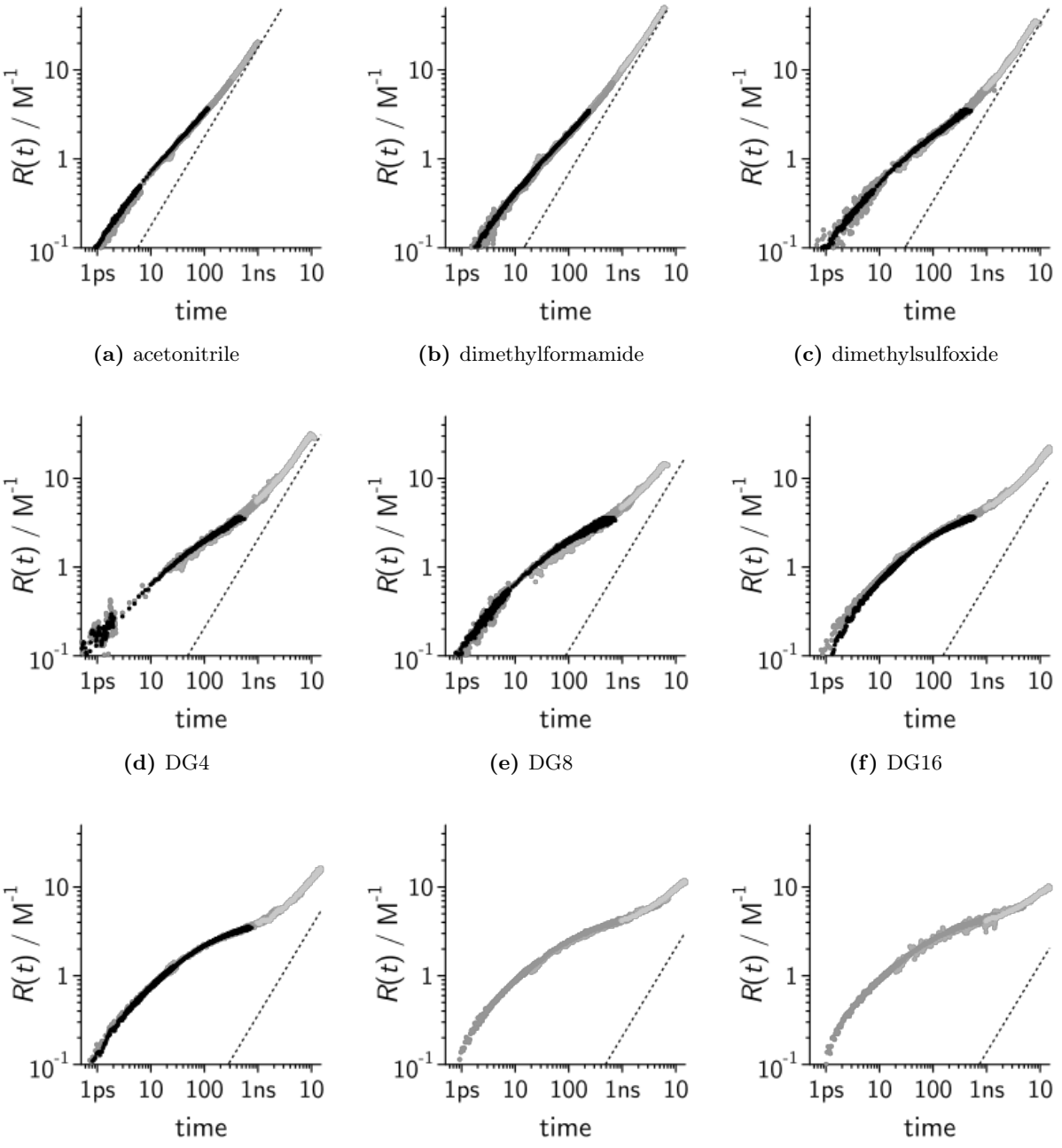

(a) acetonitrile **(b)** dimethylformamide **(c)** dimethylsulfoxide

(d) DG4 **(e)** DG8 **(f)** DG16

(g) DG32 **(h)** DG64 **(i)** DG100

Figure S 23: Universal time dependence of $R(t) = \int_0^t k(t')\mathrm{d}t'$. •... 0.8 M, •... 0.3 M, •... 0.1 M, •... 0.1 M (from TCSPC), denote the quenching dynamics at decreasing quencher concentration, with the lightest grey in the left panel indicating the TCSPC dynamics of the lowest quencher concentration. The dashed line denotes long-time asymptote given by $k_\infty t$.

13.2 Ion Kinetics - Geminate and/or Bulk?

In order to test for the participation of bulk processes on the timescale of the observed dynamics or their respective temporal onset, we performed fluence dependent ns-TA experiments. As long as the observed dynamics remain fluence independent (except for a scaling factor) they are merely governed by geminate processes. Fig. 24 shows some representative dynamics in solvents of different viscosity. These data unambiguously show that within the temporal range (a few 100 ns) studied and the applied pump fluences, F, in this work the ion dynamics are (except for a multiplicative scaling factor) completely independent of the latter.

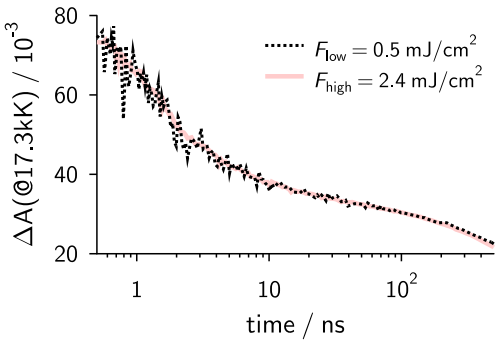

(a) Pe and 0.8 M **DMA** in dimethylformamide

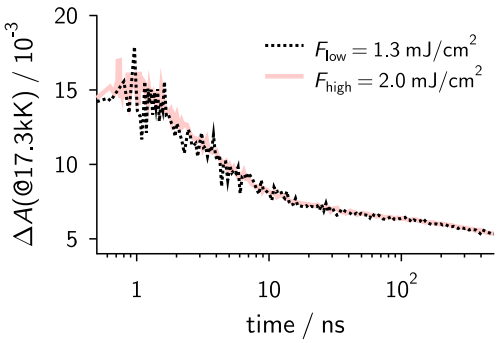

(b) Pe and 0.1 M **DMA** in dimethylsulfoxide

Figure S 24: Comparison of time-traces at the maximum of the **Pe**-anion band at different pump-fluences in (a) dimethylformamide and (b) dimethylsulfoxide. Note, that the data at lower pump fluence were multiplied by $F_{\mathrm{high}}/F_{\mathrm{low}}$.

13.3 Ion Dynamics - Spectral Changes

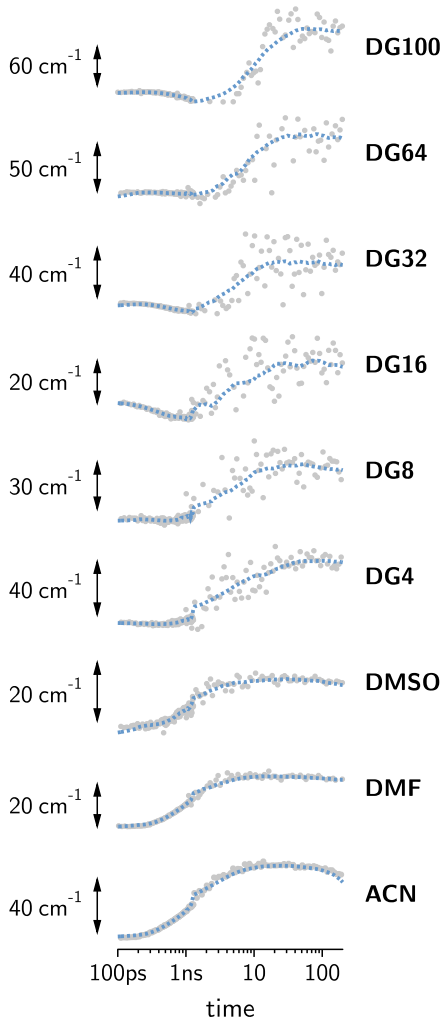

Figure S 25: Time-dependence of the first spectral moment, $E[\Delta A^1_{\mathrm{ion,n}}](t)$, of the **Pe**-anion band (from 16.5-18.5 kK) at the highest measured **DMA**-concentration.

The spectral dynamics observed in the ion pair (cf. section 10.2 and exemplified in Fig. S9b) are intriguing, as they evolve on timescales too slow to allow attributing them to processes usually responsible for spectral dynamics, such as solvation dynamics, vibrational cooling, etc.

In order to obtain a more quantitative insight into these dynamics we opted for calculating the time-dependent first moment, $E[X^1]$.[47]

$$E[X^1] = \int x^1 f(x) \mathrm{d}x \tag{S23}$$

In the case of spectral moments, x is given by the wavenumber, $\tilde{\nu}$, $f(x)$ is the area normalized TA-spectrum, $\Delta A_{\mathrm{ion,n}}$, and the integral is taken over a limited wavenumber-range covering the spectral feature of interest, i.e. the **Pe**-anion peak (16.5-18.5 kK) in our case. It is noteworthy that the data extracted from the ns-TA become less reliable the more viscous the samples are. First, the ion signal significantly decreases at long times and high viscosities (cf. Fig. 4). Second, for the two samples with highest glycerol content (i.e. DG64 and DG100) a distinct change in the **Pe**-anion band (high energy shoulder) can be observed at long times, indicating the contribution of a parasitic reaction pathway.

We can now turn to the question which process is responsible for this distinct spectral evolution. Similar dynamics had previously been observed by Asahi and Mataga[48] and attributed to the temporal changes in the spatial distribution of the ion pair. In order to test this hypothesis we calculated the temporal evolution of the first (spatial) moment of the ion pair distribution. Here, x in eqn. (S23) denotes the interparticle distance, r, and $f(x)$ is given by the ion pair distribution function, $\rho^{\mathrm{I}}(r,t)$. Fig. S26 compares the time-dependence of the spectral and spatial moments. It is evident, that, indeed, the time-scale of both processes are similar. In particular, the point at which the spatial moment overcomes the Onsager radius, r_{C}, falls approximately half-way through the spectral evolution.

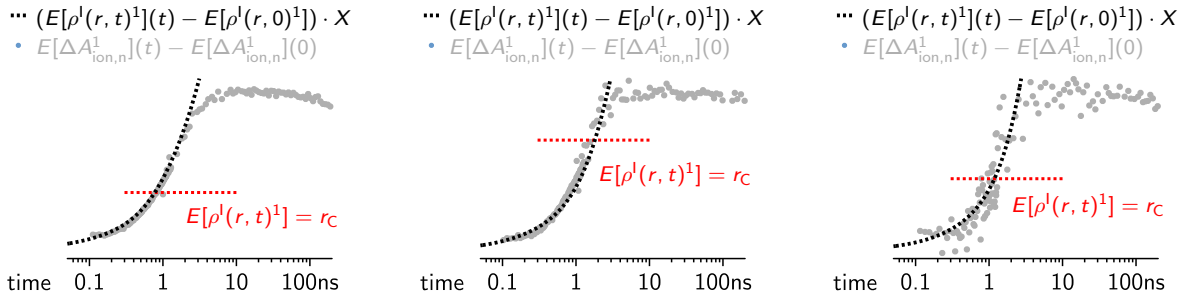

(a) acetonitrile at 0.3 M **DMA** **(b)** DMF at 0.3 M **DMA** **(c)** DMSO at 0.3 M **DMA**

Figure S 26: Comparison of the time-dependence of the first spectral moment of the **Pe**-anion with that of the first spatial moment of the ion distribution, $E[\rho^{\mathrm{I}}(r,t)^1](t)$. X denotes an arbitrary scaling factor.

14 Collected Kinetics

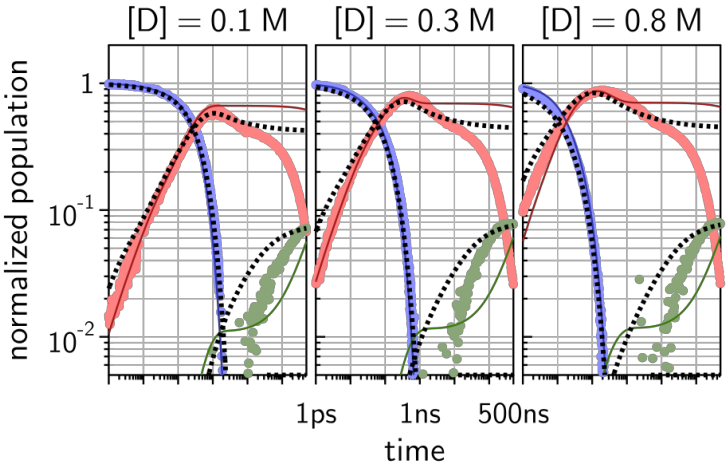

(a) acetonitrile

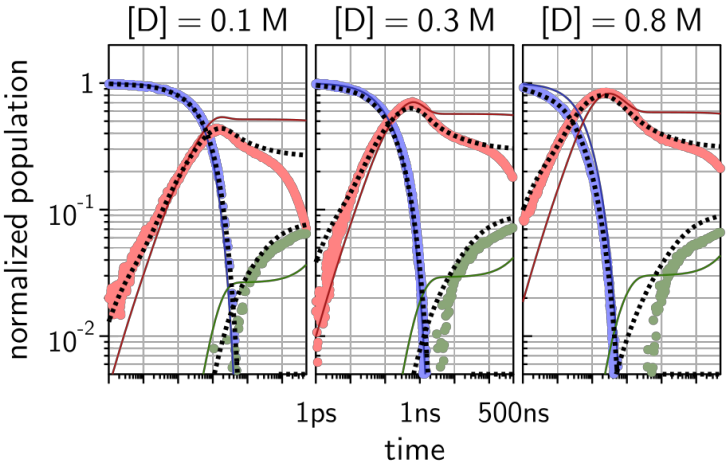

(b) dimethylformamide

Figure S 27: Kinetics in ACN and DMF. Colored markers . . . experimental data, colored lines . . . formal kinetics approach, dashed black lines . . . diffusion-reaction approach.

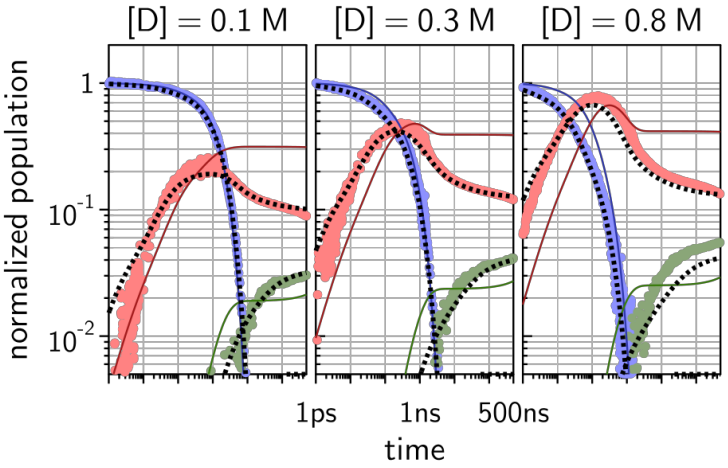

(a) dimethylsulfoxide

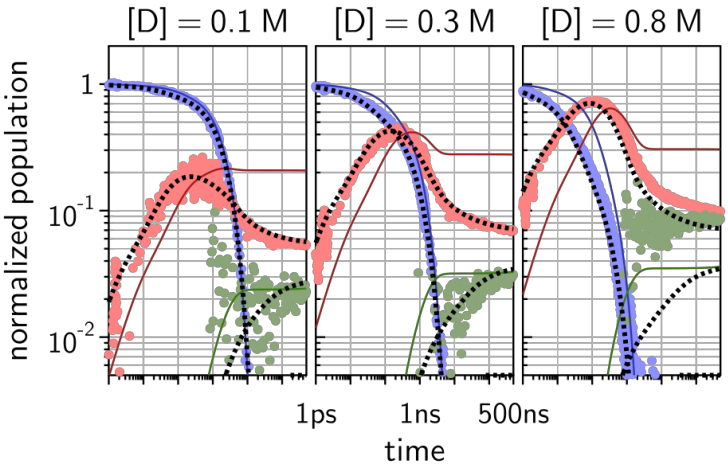

(b) DG4

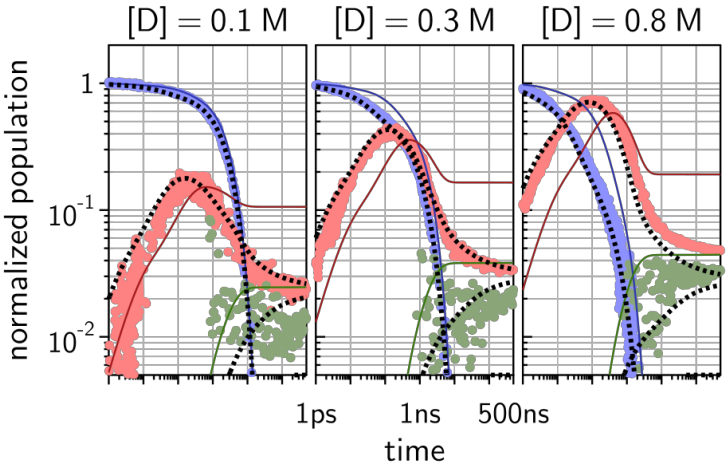

(c) DG8

Figure S 28: Kinetics in DMSO to DG8. Colored markers . . . experimental data, colored lines . . . formal kinetics approach, dashed black lines . . . diffusion-reaction approach.

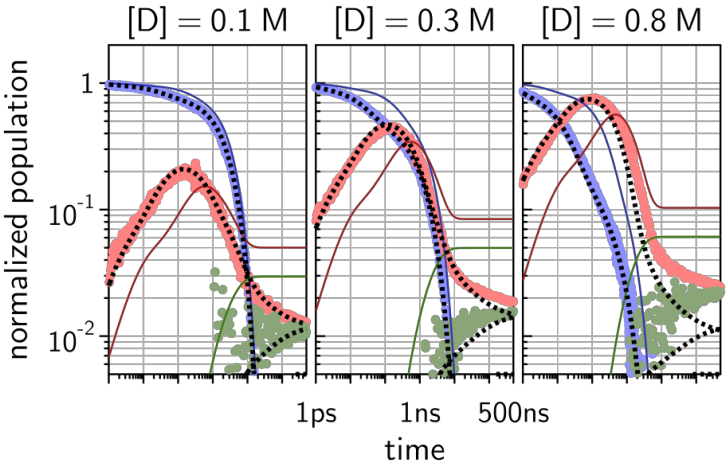

(a) DG16

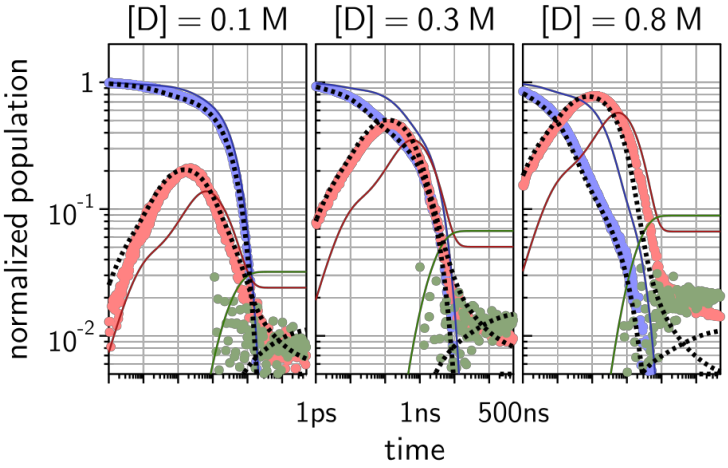

(b) DG32

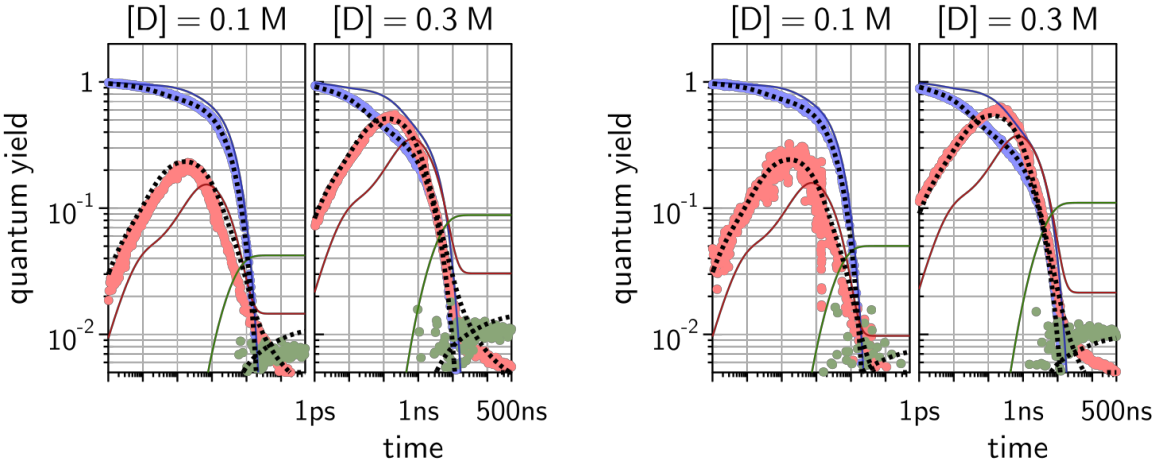

(c) DG64

(d) DG100

Figure S 29: Kinetics in DG16 to DG100. Colored markers . . . experimental data, colored lines . . . formal kinetics approach, dashed black lines . . . diffusion-reaction approach.

References

[1] D. Shoup and A. Szabo, *Biophys. J.*, 1982, **40**, 33–39.

[2] A. Rosspeintner, G. Angulo and E. Vauthey, *J. Phys. Chem. A*, 2012, **116**, 9473–9483.

[3] S. F. Swallen, K. Weidemaier and M. D. Fayer, *J. Chem. Phys.*, 1996, **104**, 2976–2986.

[4] S. F. Swallen, K. Weidemaier, H. L. Tavernier and M. D. Fayer, *J. Phys. Chem.*, 1996, **100**, 8106–8117.

[5] Y. Marcus, *The Properties of Solvents*, John Wiley & Sons Ltd., 1998.

[6] C. D. Volpe, G. Guarino, R. Sartorio and V. Vitagliano, *J. Chem. Eng. Data*, 1986, **31**, 37–40.

[7] G. Angulo, M. Brucka, M. Gerecke, G. Grampp, D. Jeannerat, J. Milkiewicz, Y. Mitrev, C. Radzewicz, A. Rosspeintner, E. Vauthey and P. Wnuk, *Phys. Chem. Chem. Phys.*, 2016, **18**, 18460–18469.

[8] A. Rosspeintner, G. Angulo and E. Vauthey, *J. Am. Chem. Soc.*, 2014, **136**, 2026–2032.

[9] B. Lang, *Rev. Sci. Instr.*, DOI: 10.1063/1.5039457.

[10] B. Lang, S. Mosquera-Vázquez, D. Lovy, P. Sherin, V. Markovic and E. Vauthey, *Rev. Sci. Instr.*, 2013, **84**, 073107.

[11] K. R. Harris, *J. Chem. Phys.*, 2009, **131**, 054503.

[12] J. Bacon and R. N. Adams, *Analytical Chemistry*, 1970, **42**, 524–525.

[13] V. Hejtmanek and P. Schneider, *J. Chem. Eng. Data*, 1993, **38**, 407–409.

[14] D. P. Valencia and F. J. González, *J. Electroanal. Chem.*, 2012, **681**, 121–126.

[15] M. Liang, A. Kaintz, G. A. Baker and M. Maroncelli, *J. Phys. Chem. B*, 2012, **116**, 1370–1384.

[16] R. Zwanzig, *J. Chem. Phys.*, 1970, **52**, 3625–3628.

[17] S. Pagès, B. Lang and E. Vauthey, *J. Phys. Chem. A*, 2004, **108**, 5741.

[18] K. Weidemaier, H. L. Tavernier, S. F. Swallen and M. D. Fayer, *J. Phys. Chem. A*, 1997, **101**, 1887–1902.

[19] K. Hirayama, *Handbook of Ultraviolet and Visible Absorption Spectra of Organic Compounds*, Springer, New York, 1st edn, 1967.

[20] Photoelectric Spectrometry Group England Staff, *UV Atlas of Organic Compounds / UV Atlas organischer Verbindungen*, Springer US, Boston, MA, 1967.

[21] I. B. Berlman, *Handbook of Fluorescence Spectra of Aromatic Molecules*, Academic Press Inc, New York, 2nd edn, 1971.

[22] M. Montalti, A. Credi, L. Prodi and M. T. Gandolfi, *Handbook of Photochemistry*, Taylor & Francis, 3rd edn, 2006.

[23] Y. H. Meyer and P. Plaza, *Chem. Phys.*, 1995, **200**, 235–243.

[24] R. Katoh, S. Sinha, S. Murata and M. Tachiya, *J. Photochem. Photobiol., A*, 2001, **145**, 23–34.

[25] R. Bensasson and E. J. Land, *Trans. Faraday Soc.*, 1971, **67**, 1904–1915.

[26] S.-A. Yamamoto, K. Kikuchi and H. Kokubun, *J. Photochem.*, 1977, **7**, 177–184.

[27] F. Lewitzka and H.-G. Löhmannsröben, *Z. Phys. Chem.*, 1990, **169**, 203–218.

[28] P. Balk, G. J. Hoijtink and J. W. H. Schreurs, *Recl. Trav. Chim. Pays-Bas*, 1957, **76**, 813–823.

[29] T. Aoyama, Y. Yamamoto and K. Hayashi, *J. Chem. Soc., Faraday Trans.*, 1989, **85**, 3353–3358.

[30] S. U. Pedersen, T. B. Christensen, T. Thomasen and K. Daasbjerg, *J. Electroanal. Chem.*, 1998, **454**, 123–143.

[31] I. Carmichael and G. L. Hug, *J. Phys. Chem. Ref. Data*, 1986, **15**, 1.

[32] A. L. Dobryakov and N. P. Ernsting, *J. Chem. Phys.*, 2008, **129**, 184504.

[33] G. Porter and M. W. Windsor, *Proc. R. Soc. London, Ser. A*, 1958, **245**, 238–258.

[34] K. H. Grellmann, A. R. Watkins and A. Weller, *J. Phys. Chem.*, 1972, **76**, 469–473.

[35] R. O. Loutfy and R. O. Loutfy, *Can. J. Chem.*, 1976, **54**, 1454–1463.

[36] C. A. Parker and T. A. Joyce, *Chem. Commun.*, 1966, 108–110.

[37] R. H. Clarke and R. M. Hochstrasser, *J. Mol. Spectrosc.*, 1969, **32**, 309–319.

[38] G. G. Hall, *Proc. R. Soc. London, Ser. A*, 1952, **213**, 113–123.

[39] R. Nurmukhametov, *Russ. Chem. Rev.*, 1966, **35**, 469.

[40] P. S. Engel and B. M. Monroe, *Adv. Photochem.*, 1971, **8**, 245–313.

[41] R. Wilcken, M. Schildhauer, F. Rott, L. A. Huber, M. Guentner, S. Thumser, K. Hoffmann, S. Oesterling, R. de Vivie-Riedle, E. Riedle and H. Dube, *J. Am. Chem. Soc.*, 2018, **140**, 5311–5318.

[42] T. Kasajima, S. Akimoto, S.-I. Sato and I. Yamazaki, *J. Phys. Chem. A*, 2004, **108**, 3268–3275.

[43] T. Kiba, S.-I. Sato, S. Akimoto, T. Kasajima and I. Yamazaki, *J. Photochem. Photobiol., A*, 2006, **178**, 201–207.

[44] A. Pigliucci, G. Duvanel, L. M. L. Daku and E. Vauthey, *J. Phys. Chem. A*, 2007, **111**, 6135–6145.

[45] A. V. Deshpande, A. Beidoun, A. Penzkofer and G. Wagenblast, *Chem. Phys.*, 1990, **142**, 123–131.

[46] B. Brüggemann, P. Persson, H.-D. Meyer and V. May, *Chem. Phys.*, 2008, **347**, 152–165.

[47] O. Braem, T. J. Penfold, A. Cannizzo and M. Chergui, *Phys. Chem. Chem. Phys.*, 2012, **14**, 3513–3519.

[48] T. Asahi and N. Mataga, *J. Phys. Chem.*, 1991, **95**, 1956–1963.